Bulletin of the Seismological Society of America. Vol. 60, No. 5, pp. 1701–1731. October, 1970

ANALYSIS OF RAYLEIGH-WAVE MULTIPATH PROPAGATION AT LASA*

By Jack Capon

ABSTRACT

An investigation has been made of the multipath propagation of Rayleigh waves by using data obtained from the large aperture seismic array (LASA). The use of the LASA in conjunction with a high-resolution analysis technique provides a greater angular resolution and accuracy than was previously possible for the analysis of the multipath propagation. Measurements have been made of this phenomenon for the Rayleigh waves of 26 events distributed at various azimuths and distances from LASA. On the basis of these measurements reasonably good conjectures are made concerning the actual propagation paths for groups in the 20- to 40-sec period range. It is shown that in almost all cases these propagation paths can be associated with refractions and reflections at the continental margins.

Introduction

A problem of considerable importance in seismology is that of distinguishing between earthquakes and underground nuclear explosions on the basis of seismic observations. There has been a considerable effort in recent years directed to this problem. This effort has led to successful results in the sense that it is now possible to discriminate between natural events and explosions, with very little error, for events which are above a certain magnitude threshold. One of the factors which has led to this success has been the use of the discriminant which is based on the relationship between the surface-wave magnitude (M_s) and the body-wave magnitude (m_b) (*cf.* Press *et al.*, 1963; Brune *et al.*, 1963; Liebermann *et al.*, 1966; Marshall *et al.*, 1966; Capon *et al.*, 1969.

The surface-wave magnitude M_s is based on the amplitude of fundamental-mode Rayleigh waves with periods of about 20 sec and is computed as recommended by Gutenberg (1945). The body-wave magnitude m_b is based on the amplitude of short-period P waves recorded at teleseismic distances and is computed as indicated by Gutenberg and Richter (1956). Thus, if the Rayleigh wave of an event can be detected along with the P wave, it is possible to distinguish whether the source is an earthquake or underground nuclear explosion with very little, if any, error. However, it should be mentioned that some doubts have been raised recently as to whether the discriminant based on $M_s - m_b$ will have diagnostic capabilities at low magnitudes which are as good as those for higher magnitudes (*cf.* Liebermann and Pomeroy, 1969). There is some evidence that this problem may be overcome by employing longer-period Rayleigh-wave energy in the computation of M_s.

Unfortunately, the Rayleigh wave of an event is not as readily detectable as the P wave of the event (*cf.* Capon, 1969a). Thus, it is the detectability of the Rayleigh wave that is limiting the identification level at which the powerful $M_s - m_b$ discriminant can be applied. It is for this reason that the determination of the properties of the Rayleigh wave is extremely important for the problem of seismic discrimination. This is especially true for those properties which aid in the detection of the Rayleigh wave.

* This work was sponsored by the Advanced Research Projects Agency of the Department of Defense.

The theory describing the propagation of Rayleigh waves in horizontally layered media is relatively well understood (*cf.* Ewing *et al.*, 1957, and Bullen, 1963). These waves travel in a dispersive mode of propagation which is characterized by a group and phase velocity that are determined by the elastic properties of the layered media. If the media contain a vertical boundary across which there is a velocity contrast, i.e., the group and phase velocities on one side of the boundary are different from those on the other side, then the dispersive wave train is refracted across the boundary according to Snell's Law for the respective phase velocities. In addition to this refraction, some of the energy of the dispersive wave train is reflected at the boundary in the usual way so that the angle of reflection is the same as the angle of incidence. The travel time along a path which crosses the boundary is determined by the group velocities in the respective media. A detailed discussion of these propagation characteristics will be given subsequently.

It is well known that the group and phase velocities for continental regions differ from those of oceanic regions, Oliver (1962). Thus, in terms of propagation of Rayleigh waves in the surface layers of the Earth the boundaries mentioned previously correspond to the continental margins which mark the transition from continental to oceanic crust. The refraction, as well as reflection, of Rayleigh waves at these continental margins will lead to extremely complex propagation paths for these waves. This fact seems to have been first established in a definitive manner by Evernden (1953), (1954). Evernden's results were based on the visual measurements of time delays, and thus phase velocity, using a tripartite array, with aperture of about 80 km, located near Berkeley, California. The multipath propagation of Rayleigh waves has also been considered by Pilant and Knopoff (1964) and Knopoff *et al.* (1966). It is interesting that, except for these latter works, very little has been done on investigating multipath propagation of Rayleigh waves since Evernden's original effort.

Evernden used a visual measurement technique for determining phase velocity. Thus, he was able to obtain the direction of approach at various time intervals along the wave train of only the particular frequency group with the dominant power. His method is, of course, subject to considerable error if there are different frequency groups of comparable power arriving at the array simultaneously from different directions, as happens very often. The purpose of the present work is to investigate the multipath propagation of Rayleigh waves using observations obtained from the large aperture seismic array (LASA) located in eastern Montana. At the time that the experiments were performed the LASA consisted of 21 subarrays of 25 short-period vertical seismometers as indicated in Figure 1. At the center of each subarray there was a three-component set of long-period seismometers oriented in the vertical, north-south and east-west directions. Only the long-period vertical (LPZ) instruments will be considered. The frequency response of these instruments is shown in Figure 2. A detailed description of the LASA has been given by Green *et al.* (1965).

The LASA data will be analyzed by means of a high-resolution frequency-wave-number spectrum analysis program described previously by Capon (1969b). The use of this program will lead to the measurement of the direction of approach of Rayleigh waves with very high angular accuracy and resolution. Thus, it will be possible to determine the angles of arrival of various frequency groups, arriving simultaneously at the array, during successive 200-sec time intervals starting at the onset time of the Rayleigh wave. Thus, unlike Evernden, it will be possible to measure group delays as well as directions of approach. The group delay will, of course, be known only in multiples of 200 sec. However, this information appears, in many cases, to be adequate

for allowing a reasonably good conjecture to be made concerning the actual paths taken by the various group arrivals at LASA. As expected, in most cases, the multipath propagation can be associated with reflections and refractions at the continental margins. However, there are some interesting examples in which the multipath propagation appears to be caused by other factors, for example, tectonic features such as ridges.

High-Resolution Analysis

The frequency-wavenumber power spectrum provides the information concerning the power as a function of frequency and wavenumber for propagating waves. Thus,

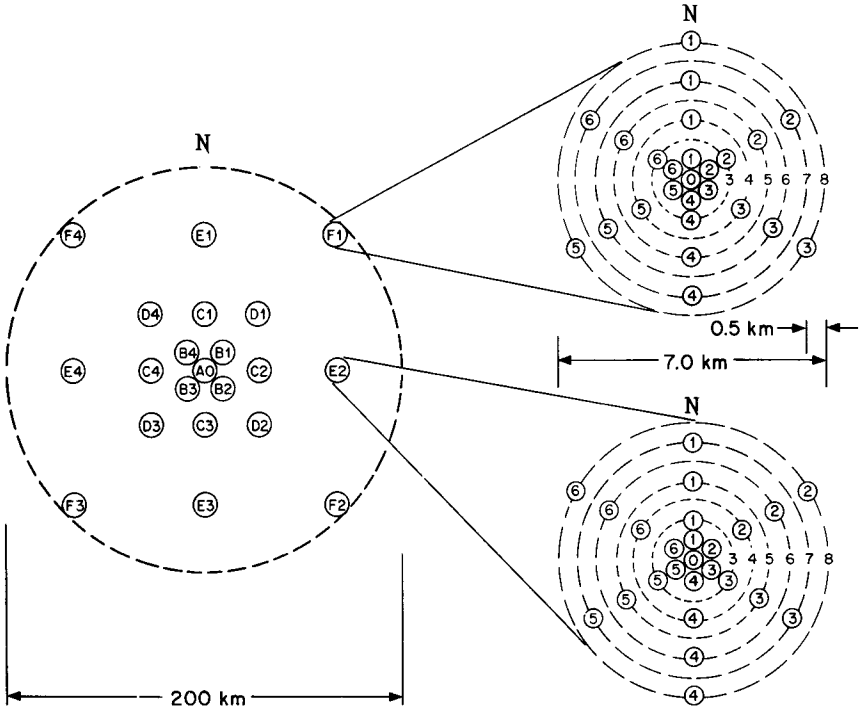

FIG. 1. General arrangement of the large aperture seismic array.

this spectrum can be used in the present work to determine the direction of approach, as well as the phase velocity and relative power of various frequency groups of a Rayleigh wave. These groups arrive at the array at different angles during different time periods along the extent of the wave train due to the multipath propagation of Rayleigh waves. It is highly desirable to determine the manner in which the angles of arrival of the various frequency groups change with time, as these data provide considerable information concerning the actual propagation paths. Thus, we are interested in the frequency-wavenumber spectrum defined, as well as measured, over relatively small time intervals. This time interval should be small enough so that during this time interval the angles of arrival do not change significantly. In addition, it should be large enough so that a reasonably good resolution in frequency between the various frequency groups is possible. It has been found experimentally that the time interval which satisfies these requirements is approximately 200 sec. Thus, the frequency-

wavenumber spectrum is measured over successive nonoverlapping 200-sec intervals of time in the present work.

The particular technique used to measure the frequency-wavenumber spectrum is the high-resolution (HR) method described in detail by Capon (1969b). This method of measurement employs a wavenumber window whose shape changes and is a function of the wavenumber at which an estimate is obtained. This window always has unity response at the wavenumber at which the estimate is obtained. As a consequence, the wavenumber resolution of the HR method is considerably better than that of conventional methods which employ a fixed wavenumber window.

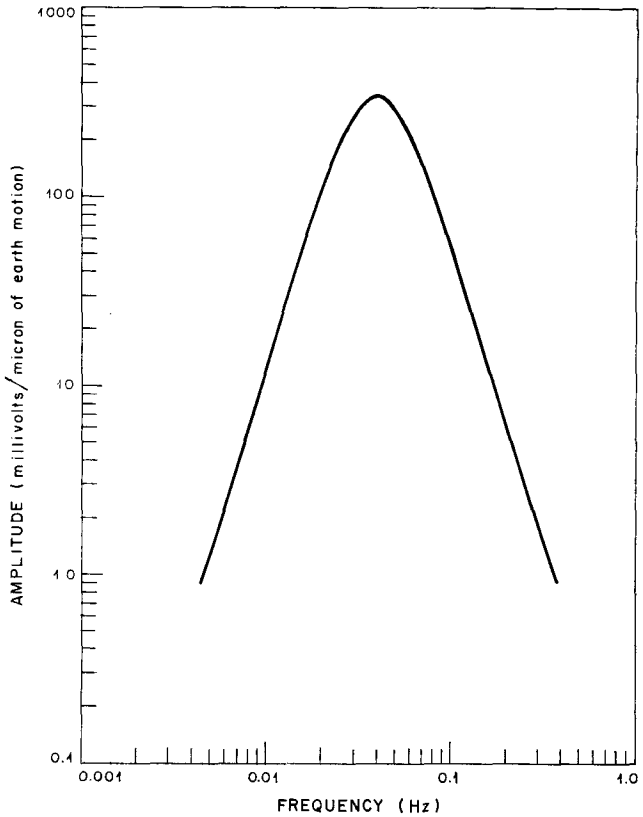

FIG. 2. Long-period system transfer function.

The HR method was used to measure the frequency-wavenumber spectrum over four successive nonoverlapping 200-sec intervals, starting at the onset time of the Rayleigh wave, so that a total of 800 sec was considered. The measurement was made at 0.025, 0.030, 0.040, 0.050 Hz, corresponding to period groups of 40, 33, 25 and 20 sec, respectively. The details of the measurement, as well as the results for a specific event, are given by Capon (1969b).

The frequency window used in the measurement is the Bartlett window shown in Figure 3 (*cf.* Blackman and Tukey, 1959). This figure may be used to determine the amount of rejection of one frequency group that is obtained when another frequency group is analyzed. For example, if the 40-sec period group is analyzed, corresponding to 0.025 Hz, the 33-sec period group, corresponding to 0.030 Hz, will have its power contribution rejected by about 3.5 db, which is the value of the window selectivity at

0.030 − 0.025 = 0.005 Hz. If the power of the 33-sec period group is about the same as, or less than, the power of the 40-sec period group, then 3.5 db is sufficient rejection; that is, in this case the measurement of the wavenumber spectrum for the 40-sec period group will not be obscured by that of the 33-sec period group. However, if the power of the 33-sec period group is larger than that of the 40-sec period group, then it is possible for the former group to obscure the measurement for the latter group. This phenomenon is called frequency windowing and is discussed extensively by Blackman and Tukey (1959). However, it is usually possible for the analyst to recognize that frequency windowing has occurred and to remove its effects in the interpretation of the measurements, as will be explained subsequently. It should be noted from Figure 3 that

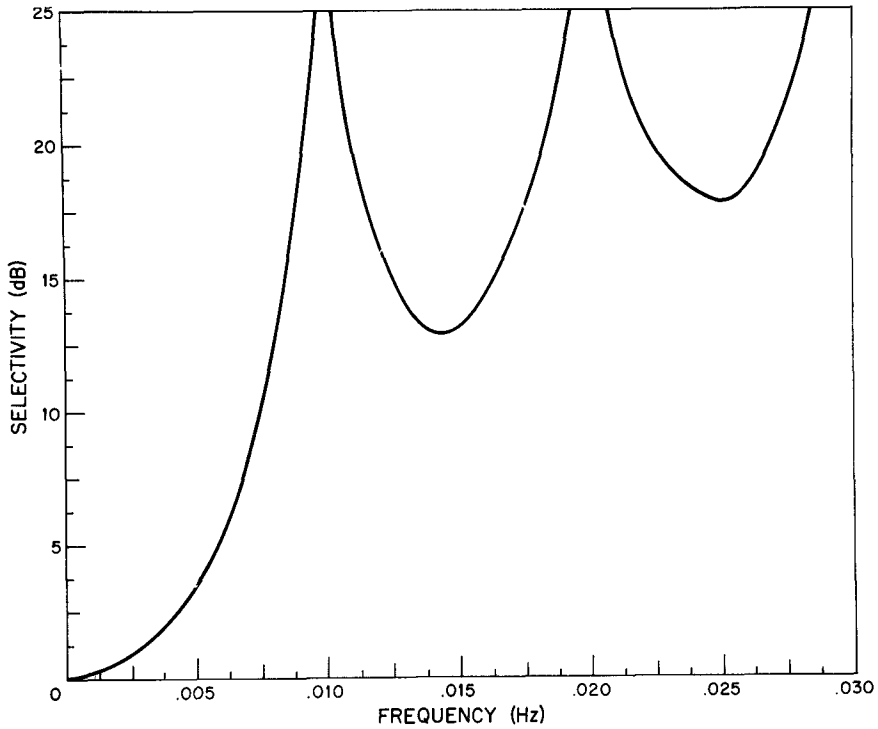

FIG. 3. Window selectivity function used in measurement.

the rejection of the power due to the 25- and 20-sec period groups is reasonably good when the 40-sec period group is analyzed.

The validity of the HR method was checked by performing a number of simulations with artificially generated data, one of which will now be described. The following dispersive wave-form sequence was defined

$$f(kT) = \sin\left[2\pi f_0 kT + \frac{1}{2}\frac{(2\pi f_1 - 2\pi f_0)}{600}(kT)^2\right],$$

$$k = 1, \cdots, 600$$

$$= 0, \text{ otherwise},$$

where f_0 , f_1 are the initial and final frequencies of the wave train and are equal to 0.025 and 0.050 Hz, respectively, and T is the sampling interval and is equal to 1 sec. The simulated signal at LASA was taken to be the sum of two such dispersed wave forms, with a delay of 200 sec between them, and with appropriate time delays inserted corresponding to the first wave arriving at LASA from an azimuth of 310° and the sec at 340°. The phase velocity was assumed to be 3.7 km/sec for each frequency group. Thus, the simulated signal in the j^{th} sensor at LASA is

$$g_j(kT) = f((k - 100 - D_{1j})T) + f((k - 300 - D_{2j})T),$$

$$k = 1, \cdots, 1000$$

$$j = 1, \cdots, 21$$

where D_{1j} , D_{2j} are delays relative to those for the sensor at AO, measured in multiples of the sampling interval T, for the arrivals from the 310°, 340° directions, respectively.

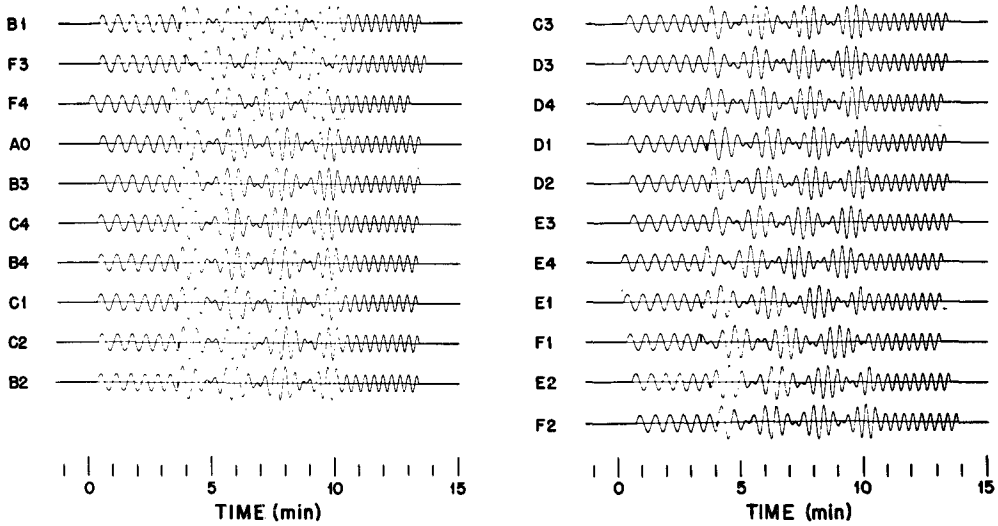

FIG. 4. Artificial wave forms used in simulation study.

The resultant wave forms are shown in Figure 4. These wave forms are supposed to be representative of the data observed on the 21 LPZ seismometers at LASA for multipath Rayleigh wave arrivals. In particular, the beating, or modulation, in the envelope of the wave trains in Figure 4 is typical of that observed for actual Rayleigh waves due to the multipath propagation (*cf.* Pilant and Knopoff 1964). It should be noted that the phase velocity, and thus the group velocity, is assumed to be nondispersive over the array in order to simplify the computation of $g_j(kT)$, and the dispersion shown in Figure 4 is attributed to propagation through dispersive media external to the array.

The results of applying the HR measurement method to these data are shown in Figures 5, 6, 7 and 8, for the period groups of 40, 33, 25 and 20 sec, respectively. The successive 200-sec measurements are depicted as a, b, c and d in these figures. The display of the results in these figures is similar to that given by Capon (1969b). The contours of constant power are displayed, in decibels relative to peak power, and in increments of 2 db from 0 to 6 db. Thus, the location of the point labeled 0 db will provide

the phase velocity of the frequency group and its angle of arrival. For example, in Figure 5a we see the 0 db point located close to the 3.5-km/sec *circle* and on the 310° azimuthal line. Hence, inspection of these figures shows that the HR method is providing an accurate indication of the angles of arrival of the frequency groups. As an

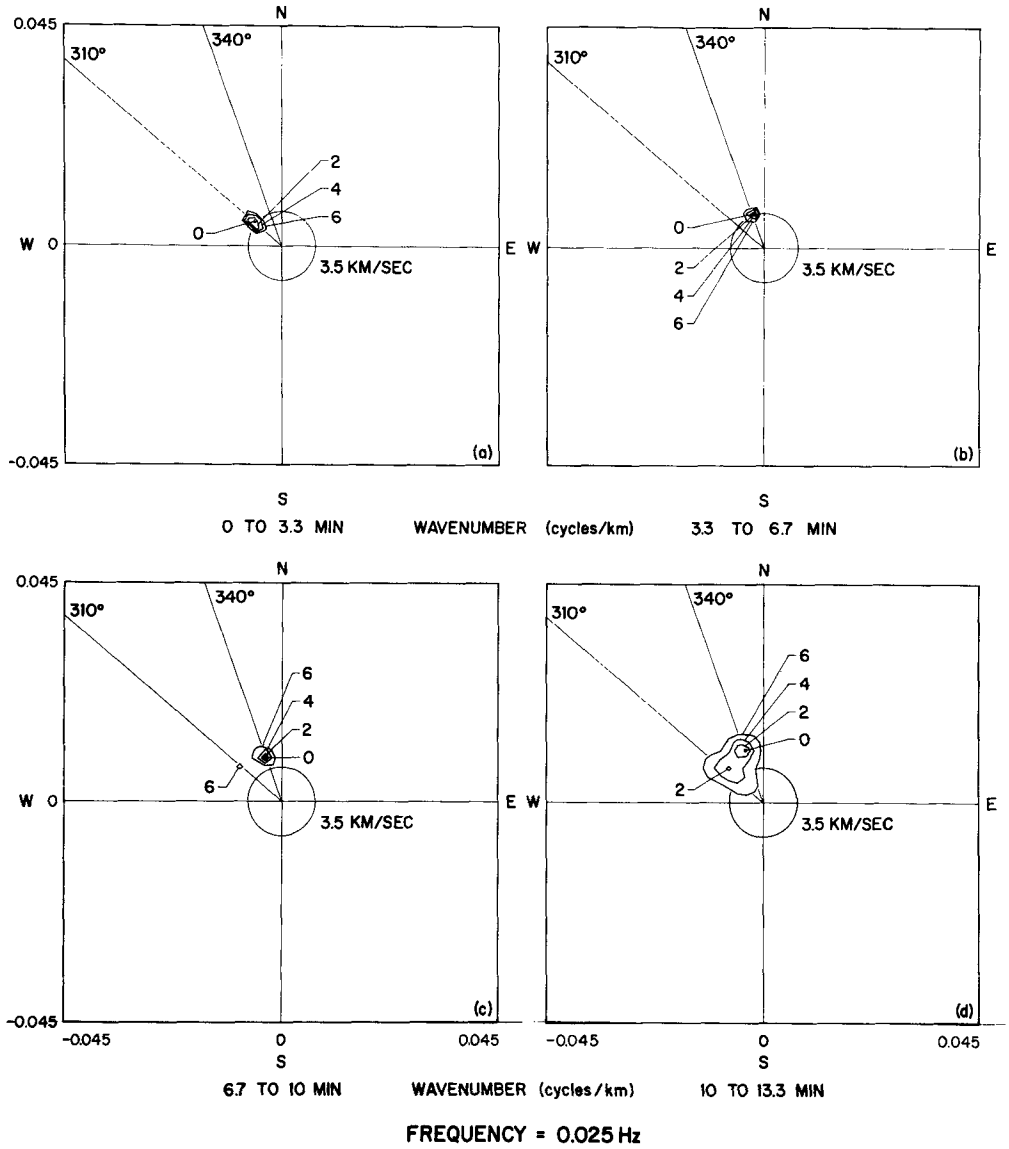

FIG. 5. High-resolution frequency-wavenumber spectra for successive 200-sec intervals of artificial wave forms at 0.025 Hz.

example, in Figure 5a we see the 40-sec period group arriving initially at an angle of 310° and then in Figure 5b the indication is that the angle of arrival is 340°.

However, frequency windowing is occurring in Figures 5c, d, 6d, 7a, and 8a and must be interpreted accordingly; that is, the power contours depicted in these figures are due to leakage through the sidelobes of the frequency window by power of frequency groups other than the one of interest (*cf.* Figure 3). It is relatively simple for the analyst to

determine that this is occurring in these figures by noting that the 0 db point is too far removed from the 3.7 km/sec velocity circle. The amount by which it is removed radially from this circle is $| f_1/v_1 - f_0/3.7 |$ cycles/km, where f_0 , f_1 are the frequencies of the desired and extraneous groups, in Hz, respectively, and v_1 is the

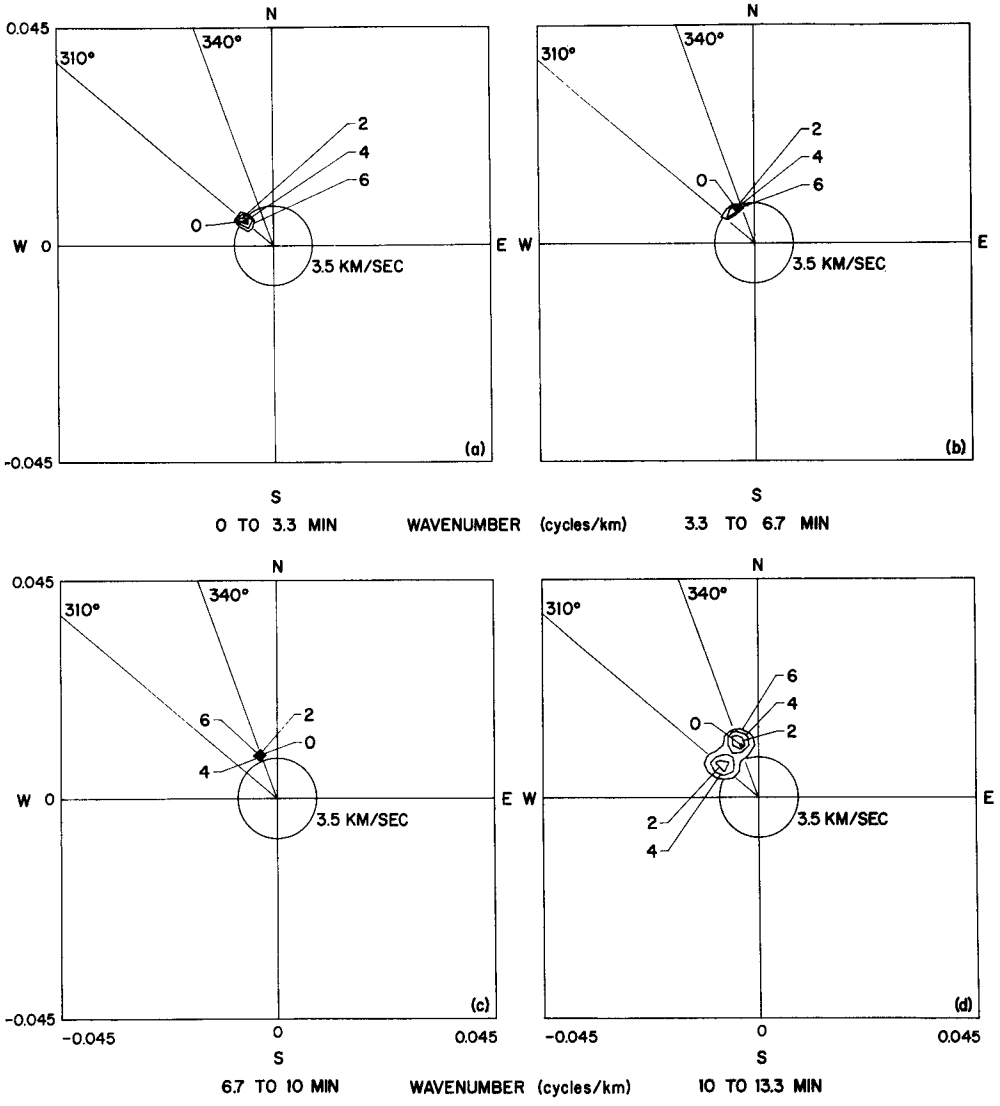

FIG. 6. High-resolution frequency-wavenumber spectra for successive 200-sec intervals of artificial wave forms at 0.03 Hz.

phase velocity, in km/sec, of the group with frequency f_1 . The frequency windowing is also observable by noting a large difference between the observed power of the desired frequency group, provided by the program, and the power of the other frequency groups, as indicated by the window in Figure 3.

The simulation results indicate that the HR method should be able to resolve two distinct peaks for two waves whose azimuthal angles of arrival are within about 5° of

each other. If a peak has been resolved, the root mean square angular error in determining the position of the peak is about 3°, as is also indicated by the simulation results. This assumes that no serious frequency windowing has occurred which can bias the measurement. If no serious frequency windowing occurs, the root mean square phase-

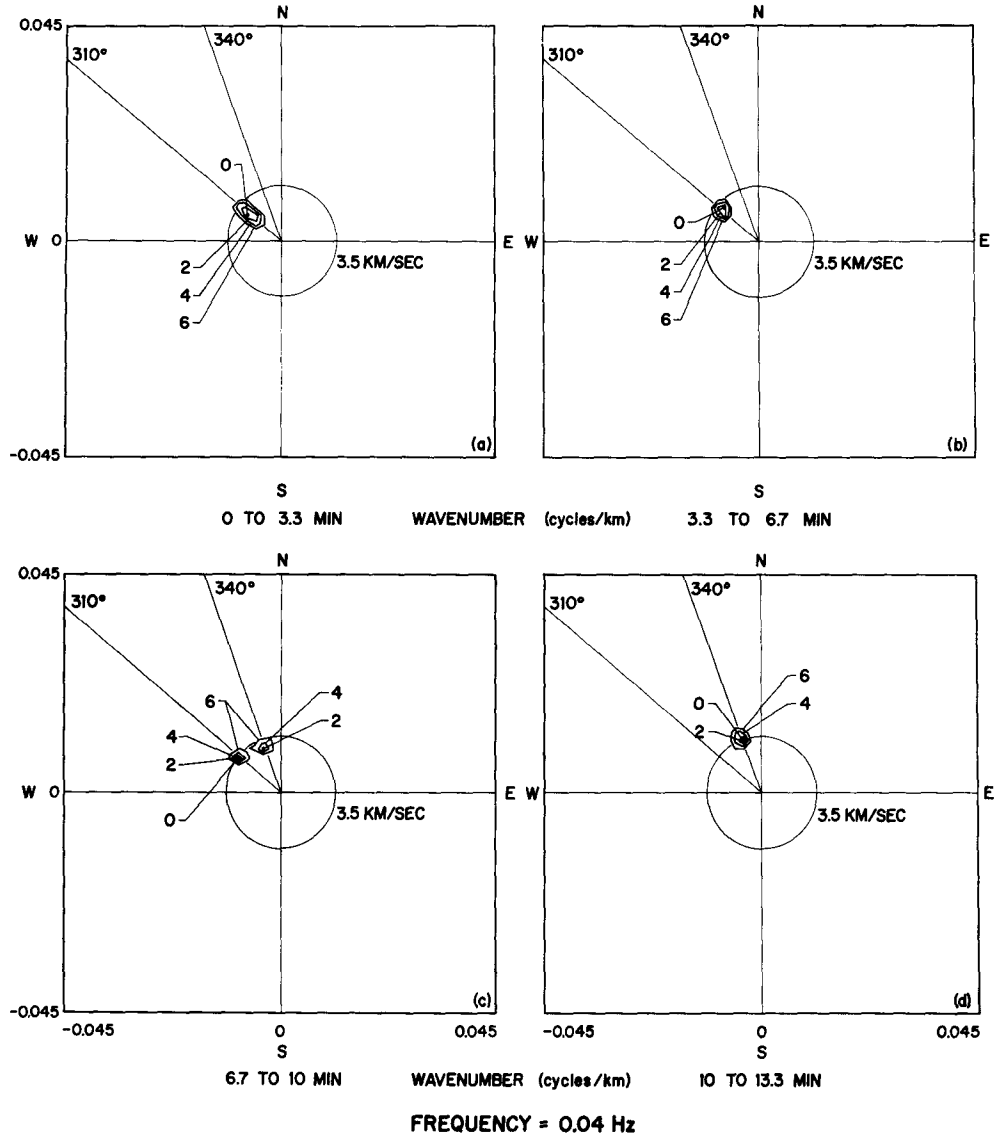

FIG. 7. High-resolution frequency-wavenumber spectra for successive 200-sec intervals of artificial wave forms at 0.04 Hz.

velocity error is about 0.2 km/sec, which is sufficient to identify all arrivals as fundamental-mode, and not higher-mode, Rayleigh waves. In addition, the root mean square error for the estimates of power appears to be about 2 db. We mention, finally, that the computer time required to obtain the multipath propagation information for an event, such as shown in Figures 5, 6, 7 and 8, is approximately 1 hr using the IBM 360/65.

Propagation Across a Boundary

A brief review will now be presented for the manner in which a dispersive wave train propagates across a boundary. We consider a ray emanating from a point A in medium 1 and intersecting the boundary at P, and then proceeding in medium 2 to a point B.

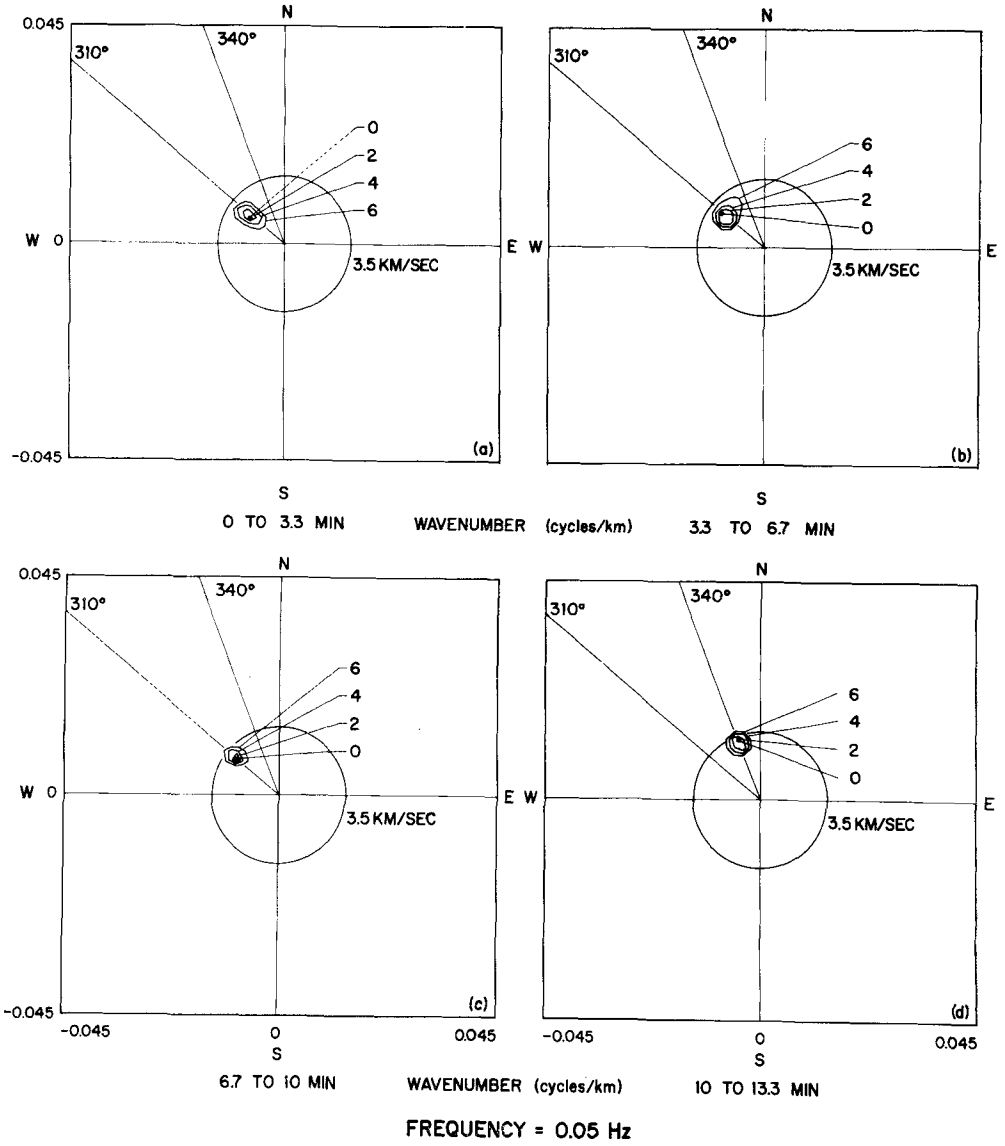

Fig. 8. High-resolution frequency-wavenumber spectra for successive 200-sec intervals of artificial wave forms at 0.05 Hz.

Let $AP = r_1$, and $PB = r_2$. The dispersive wave train in each medium can be represented by a Fourier integral with respect to the frequency ω. The contribution at B from a source at A can then be obtained by an integral over the boundary, or interface, of the excitation initiated there from the source at A.

Neglecting the effects of anelasticity, sphericity, and moving source theory, and realizing that each Rayleigh- or Love-wave mode, incident to the boundary at P, will

excite all possible Rayleigh- and Love-wave modes as well as all possible conversions, on both sides of the boundary, the Rayleigh-wave response at B, generated by a buried point source with epicenter at A, can be written

$$\sum_{i=1}^{2}\sum_{j=1}^{\infty}\sum_{k=1}^{\infty}\int\int C(\omega)e^{i\phi(\omega)}\bar{R}_{ij}(\omega, s)e^{i\bar{\psi}_{ij}(\omega,s)}D_{ijk}(\omega, s)e^{i\xi_{ijk}(\omega,s)}\exp\left[i\cdot\left(\omega t-\frac{\omega}{c_{ij}}r_1-\frac{\omega}{c_k}r_2\right)\right]d\omega ds,$$

where conversions at the boundary, to or from other than surface-wave modes, are ignored except in evaluating $D_{ijk}\exp(i\xi_{ijk})$, and s denotes the position along the interface. The index i denotes the type of the incident surface wave, Love or Rayleigh, and the index j specifies its mode number. The index k gives the mode number of the transmitted Rayleigh wave. $C\exp(i\phi)$ is the Fourier transform of the point-source time function. $R_{ij}\exp(i\bar{\psi}_{ij})$ is the function required in the plane-wave expansion to produce the radiation pattern $R_{ij}\exp(\psi_{ij})$ from the, say, double-couple point-source equivalent force system replacing the actual bilateral faulting at the focus. $D_{ijk}\exp(i\xi_{ijk})$ is the transmission coefficient applicable to ij^{th} mode incidence and k^{th} mode refraction (transmission). The quantities c_{ij} and c_k are appropriately defined phase velocities (*cf.* Harkrider, 1964, and Ben-Menaham and Harkrider, 1964).

We can rewrite the expression for the Rayleigh wave response at B as

$$\sum_{i=1}^{2}\sum_{j=1}^{\infty}\sum_{k=1}^{\infty}\int\int G_{ijk}(\omega, s)\cdot\exp\left[i\left(\omega t-\frac{\omega}{c_{ij}}r_1-\frac{\omega}{c_k}r_2+\phi(\omega)+\bar{\psi}_{ij}(\omega, s)+\xi_{ijk}(\omega, s)\right)\right]d\omega ds.$$

A number of simplifying assumptions will now be made. These assumptions appear to be in reasonable agreement with the experimental results. It will be assumed that the magnitude and phase of the Fourier transform of the point-source time function, of the radiation pattern of the source, and of the coefficient describing transmission across the boundary, are slowly varying functions of their arguments ω, s. We also assume that all Love-wave and higher-order Rayleigh-wave modes may be neglected so that the major contribution to the integral is due to the fundamental-mode Rayleigh wave. Thus, the integral will have a dominant contribution at stationary values of the exponential with respect to both ω and s. This condition is met if

$$\frac{1}{c_1'}\frac{\partial r_1}{\partial s}+\frac{1}{c_2'}\frac{\partial r_2}{\partial s}=0$$

and

$$r_1\frac{\partial}{\partial\omega}\left(\frac{\omega}{c_1'}\right)+r_2\frac{\partial}{\partial\omega}\left(\frac{\omega}{c_2'}\right)-t=0,$$

where c_1' and c_2' are the phase velocities for the fundamental-mode Rayleigh wave in medium 1 and 2, respectively.

The space derivatives $\partial r_1/\partial s$ and $-\partial r_2/\partial s$ are equal to the sines of the angles of

incidence and refraction, respectively, so that the first equation yields

$$\frac{\sin \theta_1}{c_1'} = \frac{\sin \theta_2}{c_2'},$$

which is Snell's Law and states that a dispersive wave train is refracted across a boundary according to Snell's Law for the respective phase velocities. The group volocity U_1 may be expressed as

$$1/U_1 = \frac{\partial}{\partial \omega}\left(\frac{\omega}{c_1'}\right)$$

and similarly for U_2 so that

$$t = \frac{r_1}{U_1} + \frac{r_2}{U_2}.$$

This equation states that the travel time from A to B is determined by the group velocities in the respective media, the distances r_1 and r_2 being determined by the equation given previously for Snell's Law of refraction.

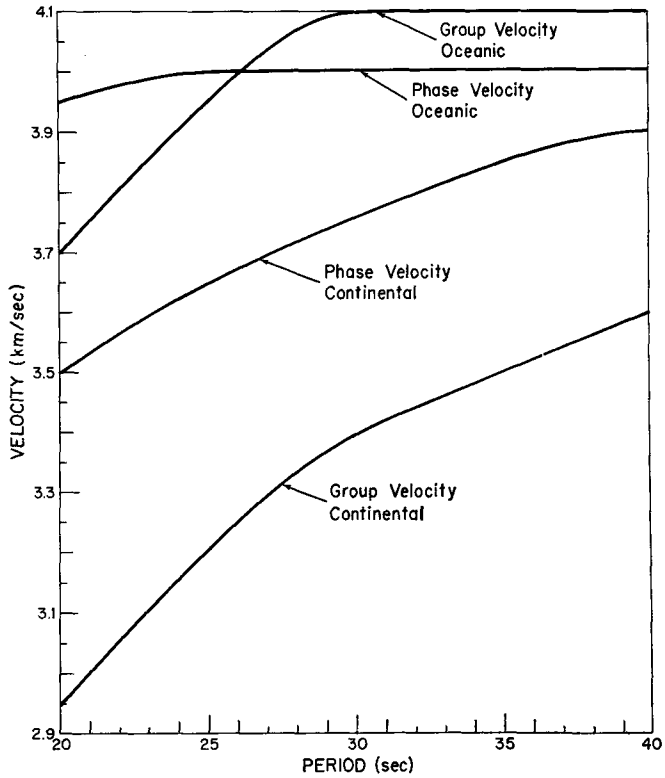

FIG. 9. Rayleigh-wave dispersion curves in the 20- to 40-sec period range.

It is also known that the ray path must satisfy Fermat's principle; that is, the ray path must be a stationary-time path. For Rayleigh waves this means that the path for the initial arrivals will be a minimum-time path while later arrivals propagate along paths which, while not minimum-time paths, are stationary-time paths. In other words,

there are usually many possible paths which can be stationary-time paths, as will be seen subsequently in the interpretation of the experimental results for the multipath propagation of surface waves.

The phase- and group-velocity curves for Rayleigh waves for continental and oceanic regions are shown in Figure 9, and were obtained from Oliver (1962). It is seen from this figure that both the phase and group velocities for oceanic regions are larger than those for continental regions at all periods. In addition, the phase velocity for the longer periods, about 40 sec, is almost the same for both continental and oceanic regions. Thus, very little refraction of those longer-period groups would be expected. This is also borne out in the experimental results to be presented subsequently. The data in Figure 9 were used to compute the amount of time saved by a group by traveling an oceanic path, of a certain distance, relative to a continental path of the same distance. The

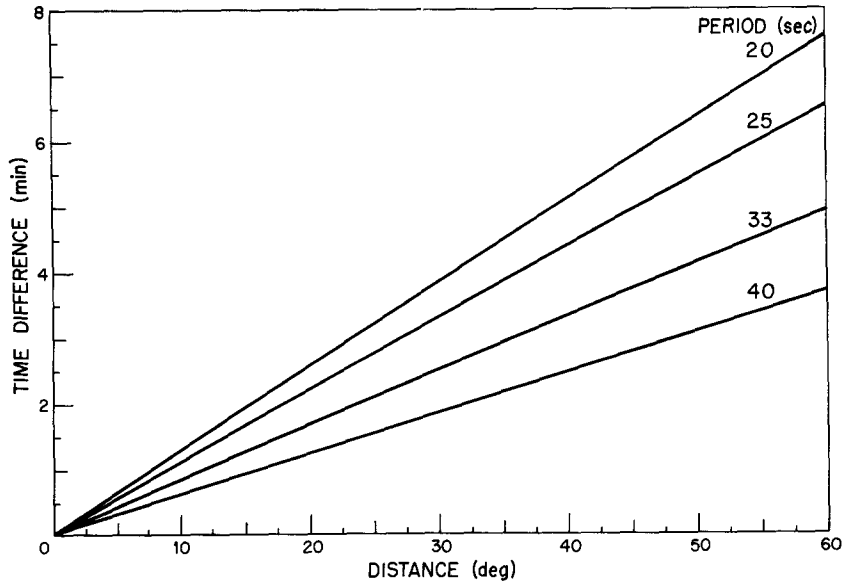

FIG. 10. Time difference for propagation in oceanic region relative to continental region.

results are given in Figure 10. This figure will be important subsequently in the attempt to correlate specific paths with observed angles of arrival and group delays.

In addition to the refraction at a boundary, there is also energy which is reflected in such a way that the angle of reflection is equal to the angle of incidence. A critical angle of incidence is reached when $c'_2 > c'_1$ and is the angle at which much of the energy is reflected. This condition is achieved at a continent-to-ocean boundary and the critical angle is given by

$$\theta_c = \sin^{-1}\left(\frac{c_c}{c_o}\right),$$

where c_c , c_o are the continental and oceanic phase velocities, respectively. The data in Figure 9 were used to compute the critical angle versus period and the results are shown in Figure 11.

The exact solutions for the reflected and transmitted Rayleigh waves are difficult to obtain. The mathematical formulation of the problem is complicated by the difficulty

of finding an elementary coordinate system in which to describe both the solutions of the wave equation and the boundary conditions. The basic difficulty arises because of the complex geometry of a free surface with relatively sharp corners. However, approximations may be used for the special case of normal incidence to obtain reflection and transmission coefficients for Rayleigh waves (*cf.* Mal and Knopoff, 1965 and McGarr and Alsop, 1967).

Analysis of Multipath Propagation

The HR method described previously was used to analyze the multipath propagation of the Rayleigh waves of 26 events. These events were observed on the LPZ seismometers at LASA and the data were recorded in digital format on magnetic tape. The locations, origin times, and other parameters obtained from USCGS for the 26 events used in the study are presented in Table 1. The locations of the epicenters of these events are shown in Figure 12 along with the observed variations in azimuth of arrival. The map shown in this figure is an equidistant azimuthal projection with LASA as the projection point. Thus, on this map all great circle paths passing through LASA appear as straight lines and all points at the same distance from LASA project on a circle centered on LASA.

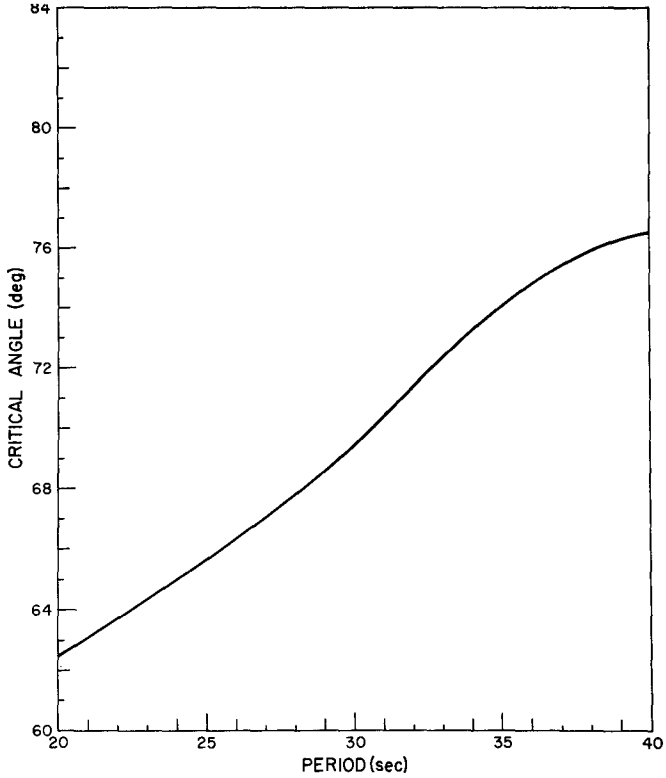

Fig. 11. Critical angle of reflection versus period at a continent-to-ocean boundary.

The wave forms for event no. 1 which occurred on November 21 1966 in the Kurile Islands are shown in Figure 13. The resemblance should be noted between these wave forms and the artificially generated wave forms, shown in Figure 4, which were used in the simulation study mentioned previously. The results obtained for the processing of

TABLE 1

LIST OF EVENTS

Event No.	Date	Region	Origin Time (GMT)	Latitude (deg)	Longitude (deg)	Distance (deg)	Azimuth (deg)	Depth (km)	Body-Wave Magnitude (USCGS)
1	21 Nov 66	Kurile Islands	12:19:27	46.7 N	152.5 E	64.3	311.5	40	5.6
2	20 Jan 67	Mongolia	01:57:23	48.0 N	102.9 E	82.3	340.7	33	6.1
3	2 Mar 67	Ecuador	02:47:32	0.3 S	78.7 W	52.7	144.5	121	5.8
4	7 Apr 67	Turkey	18:33:31	37.4 N	36.2 E	89.8	29.1	39	5.0
5	13 Apr 67	Guerrero, Mexico	19:59:52	18.5 N	100.2 W	28.6	168.0	86	5.6
6	27 May 67	Kashmir-Sinkiang Border Region	19:05:49	36.1 N	77.8 E	97.5	356.7	35	5.4
7	3 June 67	Kodiak Island Region	09:08:56	58.4 N	151.2 W	29.2	310.3	32	5.5
8	14 June 67	Tonga Islands	05:06:16	15.2 S	173.6 W	86.2	243.3	11	5.9
9	22 June 67	Andreanof Islands, Aleutian Islands	15:36:39	51.8 N	176.8 W	44.8	303.5	54	5.3
10	4 Aug 67	Central Mid-Atlantic Ridge	06:01:10	7.4 N	36.3 W	70.9	99.7	33	5.0
11	15 Aug 67	E. Russia-N.E. China Border Region	15:36:07	44.8 N	132.4 E	75.3	321.1	33	5.3
12	8 Sep 67	Near Coast of Northern Chile	08:59:59	23.4 S	70.7 W	76.8	146.8	33	5.5
13	8 Sep 67	East of Severnaya Zemlya	12:44:45	78.2 N	126.3 E	51.4	347.9	33	4.5
14	8 Sep 67	West Caroline Islands	22:34:40	12.2 N	140.8 E	96.3	295.1	27	5.3
15	13 Sep 67	Near Islands, Aleutian Islands	18:41:15	52.7 N	172.5 W	50.3	308.6	34	5.7
16	20 Sep 67	Tristan Da Cunha Region	19:46:43	34.1 S	14.6 W	114.9	113.9	33	5.2
17	22 Sep 67	Central Mid-Atlantic Ridge	08:08:04	0.7 S	20.1 W	87.8	93.3	33	5.3
18	9 Oct 67	North Atlantic Ridge	08:27:05	19.4 N	46.2 W	55.7	98.0	33	4.9
19	15 Oct 67	Near Coast of Nicaragua	08:00:50	11.9 N	86.0 W	38.7	147.2	162	6.2
20	24 Dec 67	Jan Mayen Island Region	04:22:01	71.9 N	0.9 W	50.8	22.9	33	5.0
21	11 Jan 68	South Pacific Cordillera	18:24:52	55.2 S	130.4 W	103.5	194.0	33	4.6
22	19 Jan 68	Solomon Islands	06:04:38	9.4 S	158.4 E	100.4	267.4	33	6.0
23	29 Jan 68	Easter Island Cordillera	09:16:31	24.0 S	115.7 W	70.9	189.2	33	5.0
24	25 Apr 68	Northern Easter Island Cordillera	11:28:30	8.9 S	108.8 W	55.4	183.1	33	4.8
25	21 May 68	Hokkaido, Japan Region	04:11:25	41.1 N	143.5 E	73.0	312.0	33	5.5
26	8 Sep 68	Tuamotu Archipelago Region	18:59:59	21.8 S	139.2 W	74.4	211.7	0	4.7

this event with the HR method are shown in Figures 14, 15, 16, and 17 for the period groups of 40, 33, 25 and 20 sec, respectively. The resemblance should be noted between the results shown in these figures and those in Figures 5, 6, 7 and 8 for the simulation study described previously. The occurrence of frequency windowing in Figures 14b, c, d, 15c, d and 17a should be noted. This windowing is similar to that which occurred in the simulation results described previously. Hence, the resemblance between the simu-

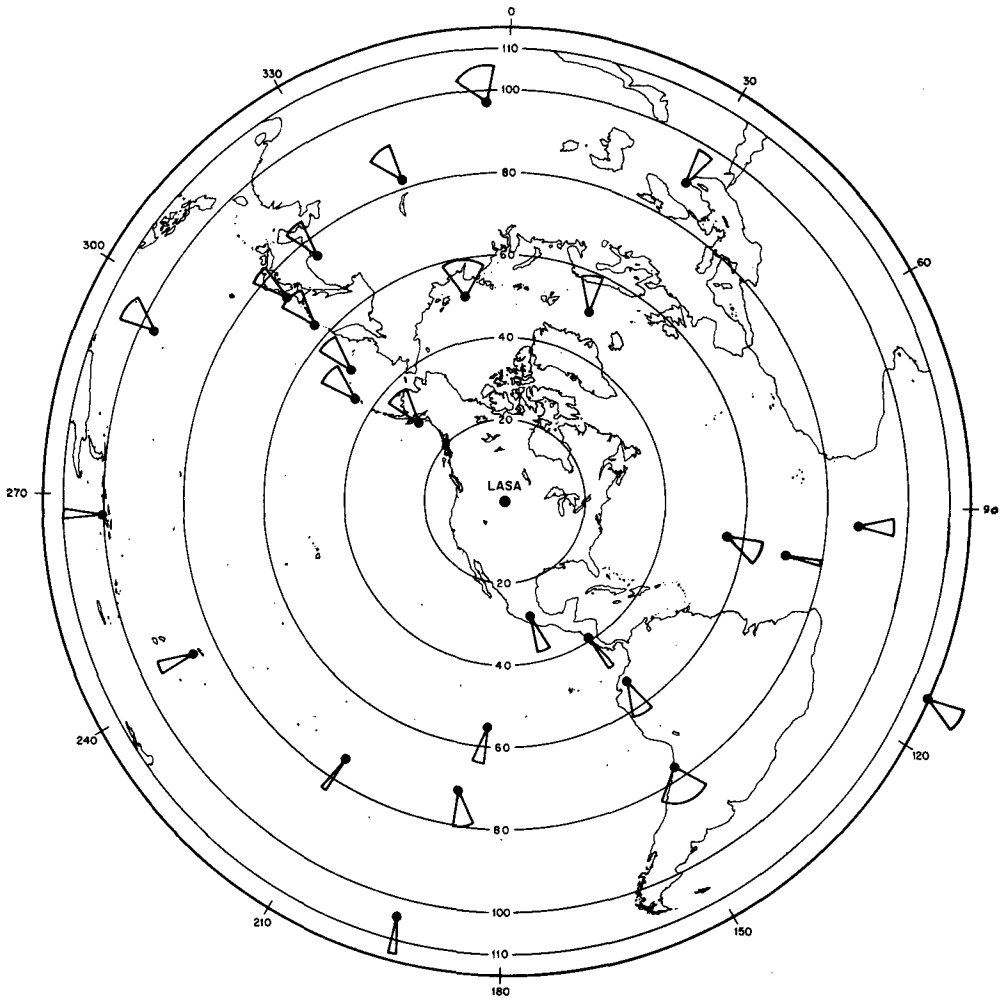

FIG. 12. Variations in azimuth of arrival of Rayleigh waves at LASA.

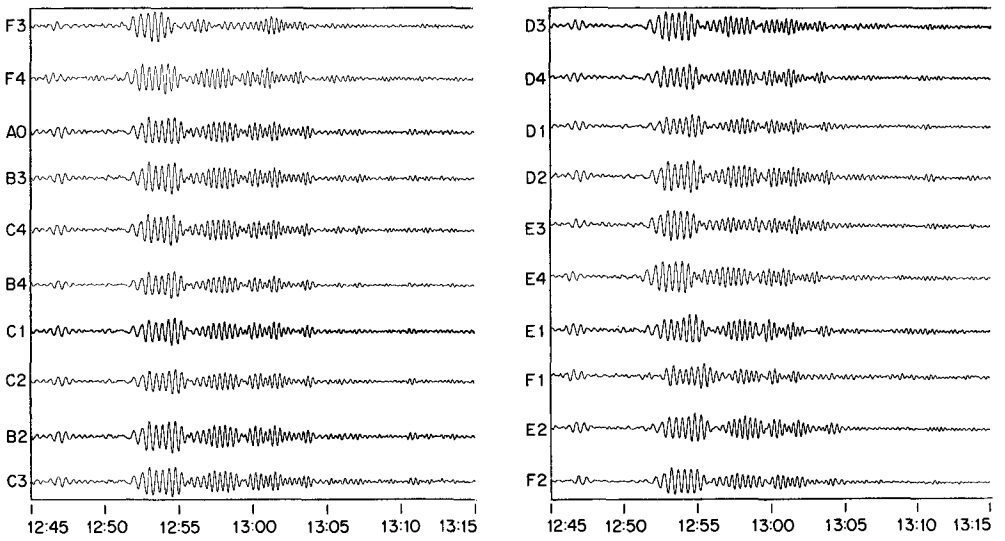

FIG. 13. The long-period wave forms for the Kurile Islands event no. 1 of November 21 1966.

lation results and those obtained with actual data lead to a reasonable amount of confidence in the measurement method, which, it should be stated, is a new technique.

The measurements made on the 26 events, such as shown in Figures 14, 15, 16 and 17 for event no. 1, were analyzed to obtain the data given in Table 2. This table lists the

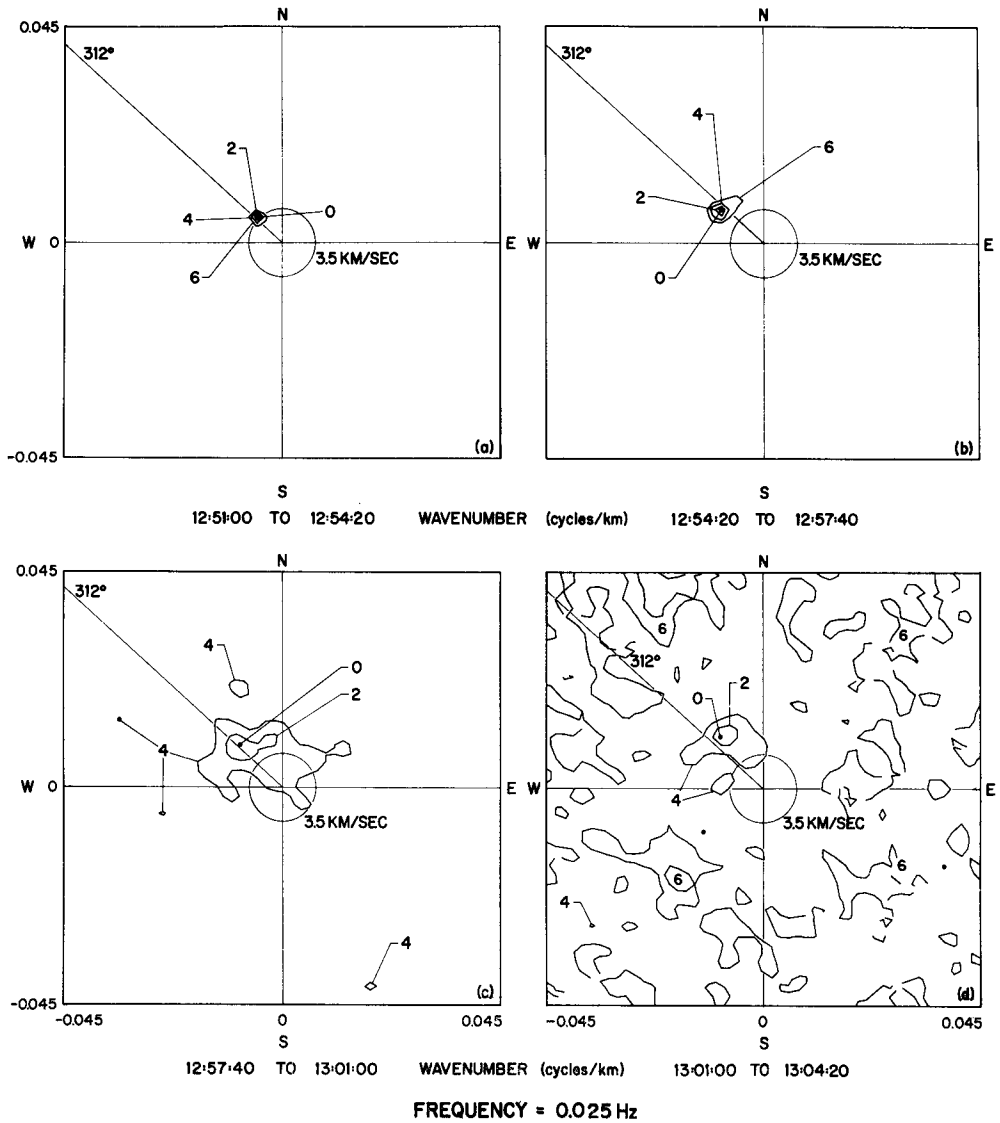

FIG. 14. High-resolution frequency-wavenumber spectra for successive 200-sec intervals of event no. 1 at 0.025 Hz.

deviation of the azimuth of arrival from the true azimuth, in degrees, of the four groups considered, during successive 200-sec intervals of time starting with the onset time of the 40-sec period group of the Rayleigh wave. In all cases this onset time was in agreement with the known origin time of the event and the propagation time computed from the group velocity and distance appropriate to the propagation path for the 40-sec period group. In Table 2 the power levels of the groups are given in decibels

relative to the power level of that frequency group which had the largest power level observed during the entire 800-sec analysis time. This power level is measured as the power output of a narrow-band filter whose selectivity function corresponds to the Barlett window shown in Figure 3. Thus, the power levels given in Table 2 enable us to

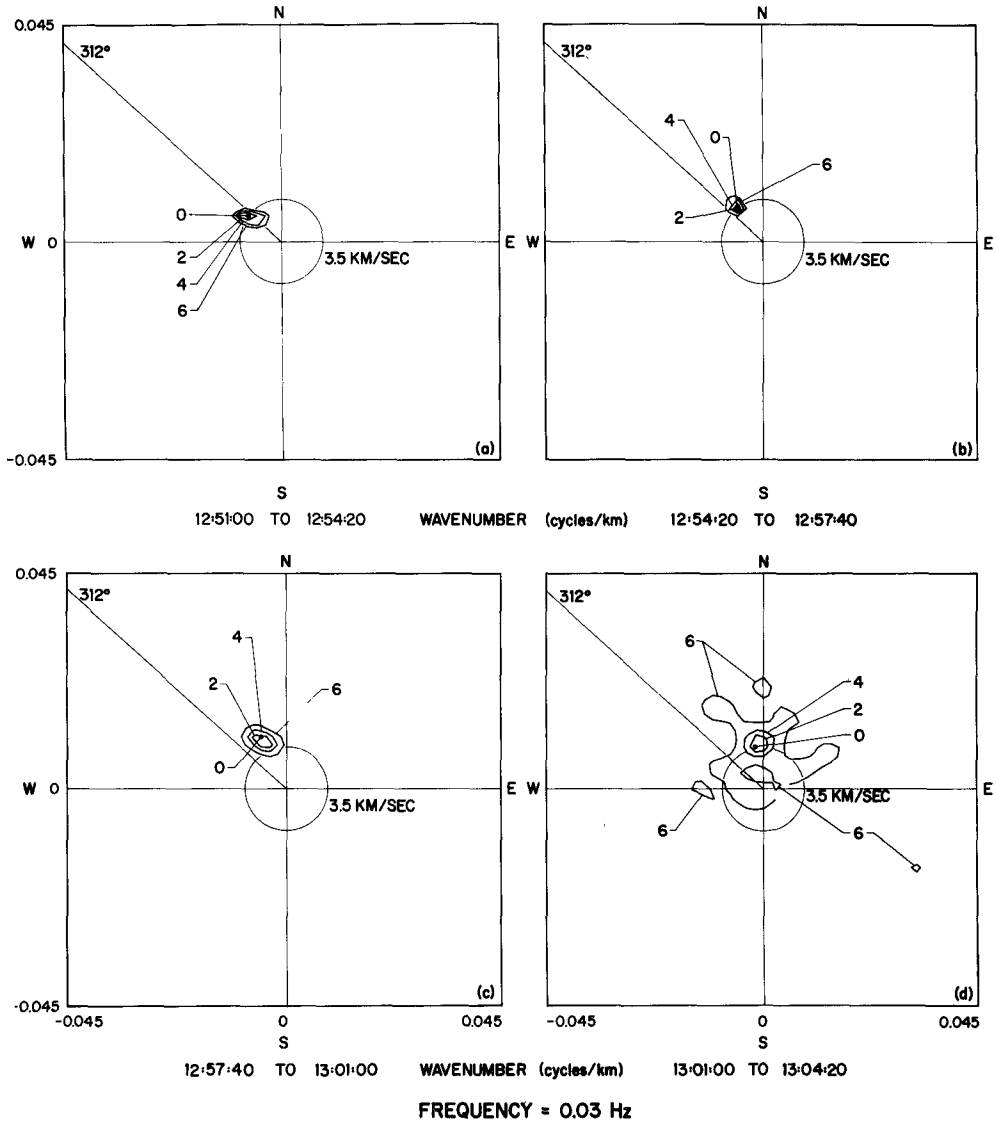

FIG. 15. High-resolution frequency-wavenumber spectra for successive 200-sec intervals of event no. 1 at 0.03 Hz.

determine the relative energies of the various group arrivals at LASA. A dash in Table 2 indicates that the group was not detected during that time interval. The data in Table 2 will be used subsequently to make conjectures about the actual ray paths for the multipath propagation of Rayleigh waves.

The azimuthal variations observed for the events are listed in Table 3. The average azimuthal difference between the extremes observed is about 33°. These data are in

reasonable agreement with the observations of Evernden (1953), (1954). However, there are discrepancies between the azimuthal variations for an event at a given location as measured by Evernden and in the present work. These differences can easily be ascribed to the difference in locations of the arrays employed, and the different meas-

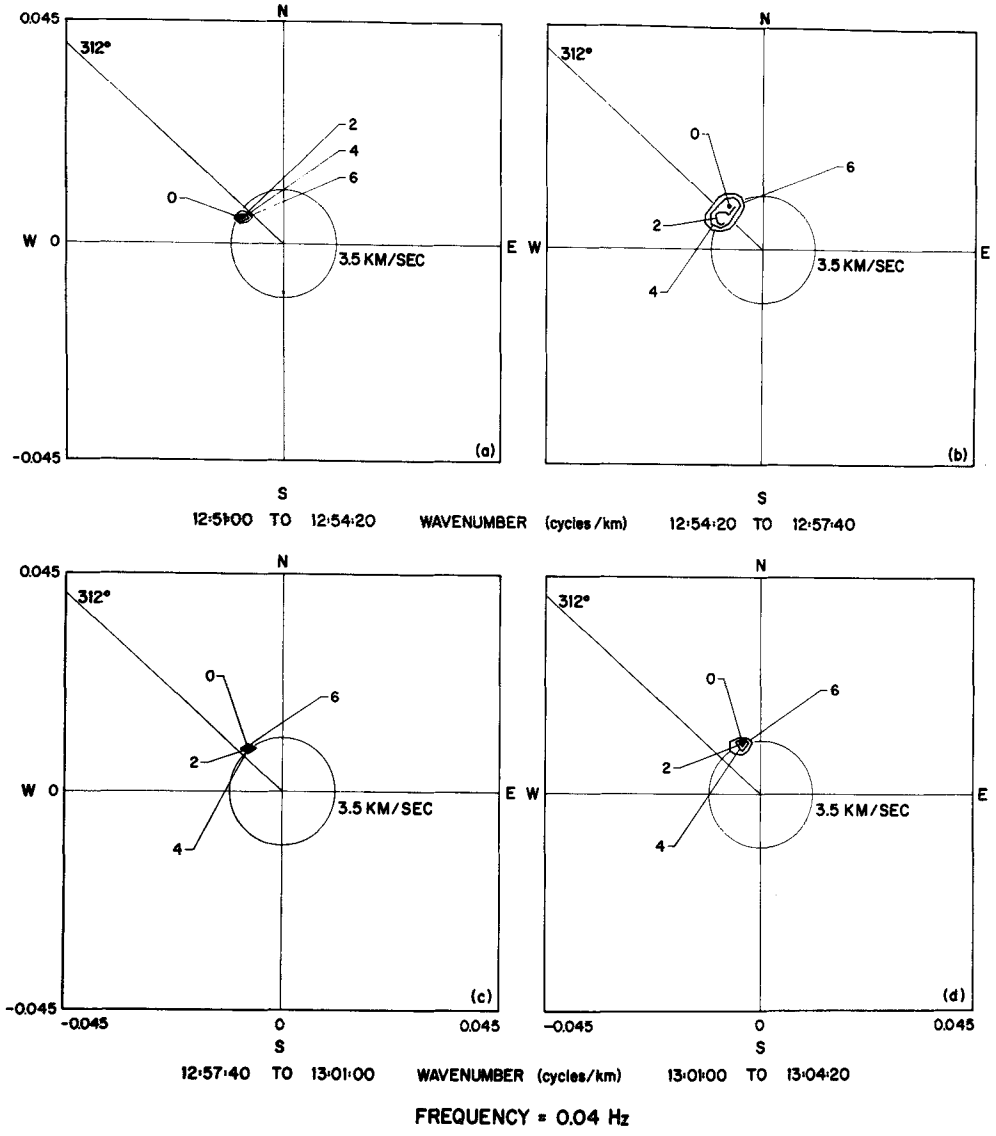

FIG. 16. High-resolution frequency-wavenumber spectra for successive 200-sec intervals of event no. 1 at 0.04 Hz.

urement methods. In addition, Evernden's measurements included periods as small as 13 sec, whereas the smallest period observed in the present work was 20 sec.

It is known that the particle motion associated with fundamental-mode Rayleigh-wave propagation should be retrograde elliptical in the plane containing the lines which are vertical and radial to the propagation path. Thus, the phase of the signal observed on a seismometer oriented in the radial direction will lead that of a signal observed on a

seismometer oriented in the vertical direction by approximately 90°. The precise value of this phase angle will be determined by the particular crustal structure at LASA. In order to check that the particle motion was correct the outputs of the seismometers oriented in the east-west and north-south directions were combined to produce a radial

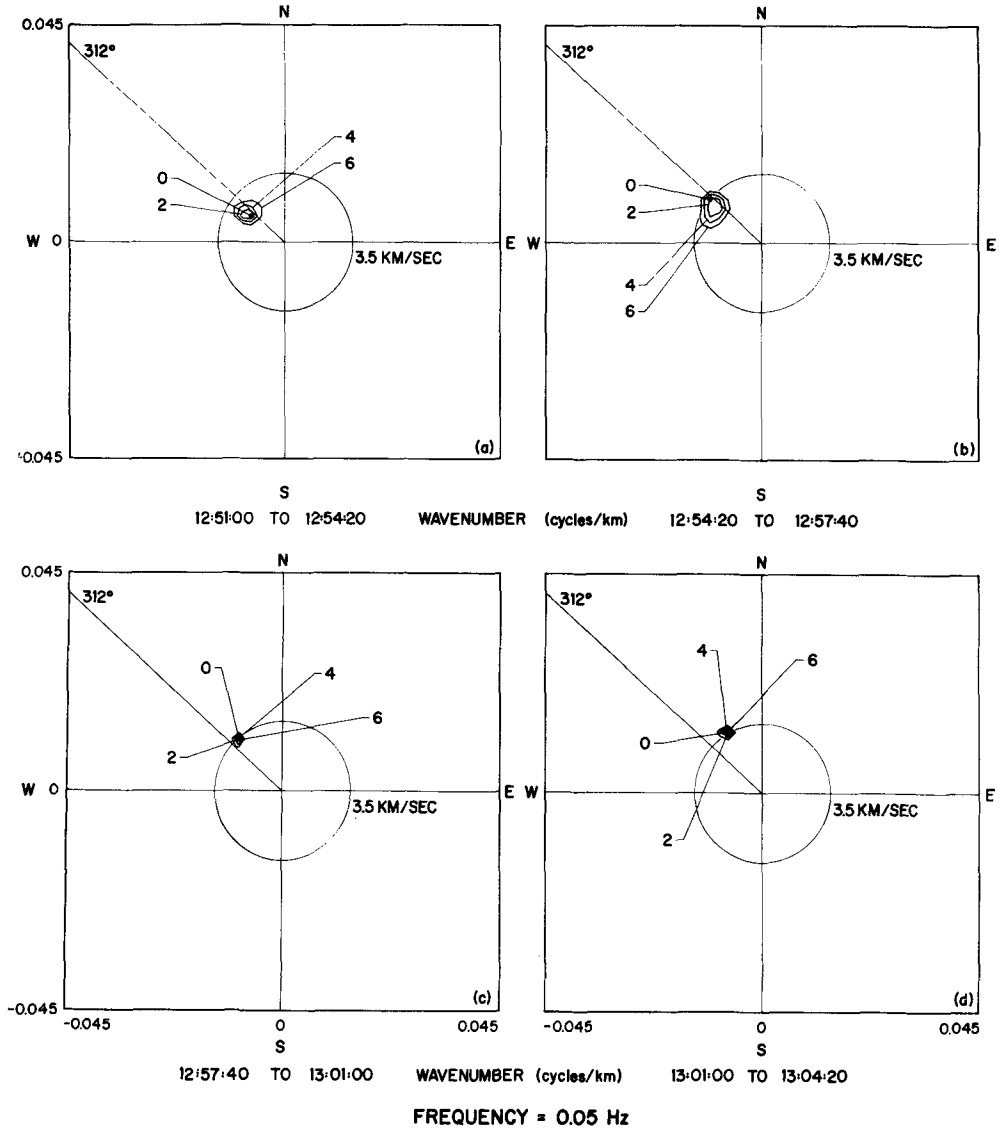

FIG. 17. High-resolution frequency-wavenumber spectra for successive 200-sec intervals of event no. 1 at 0.05 Hz.

trace for several events. The phase relationship between this trace and the vertical trace was approximately correct during the first few hundred seconds of the Rayleigh wave train. However, the phase relationship could not be checked at later times due to the multiple path propagation of the shorter-period groups. However, the check which was made is sufficient to establish the correct particle motion for Rayleigh waves.

TABLE 2

MEASURED VARIATIONS IN AZIMUTH OF ARRIVAL, AND POWER LEVELS AT VARIOUS TIMES FOR EVENTS

Event No.	Time (sec)	Azimuthal Deviations*				Power Levels†			
		At 40 sec (deg)	At 33 sec (deg)	At 25 sec (deg)	At 20 sec (deg)	At 40 sec (db)	At 33 sec (db)	At 25 sec (db)	At 20 sec (db)
1	0–200	0	−5	−11	—	7	6	0	—
	200–400	—	11	11	−12	—	8	2	7
	400–600	—	—	11	10	—	—	5	4
	600–800	—	—	30	18	—	—	12	5
2	0–200	0	0	—	—	5	5	—	—
	200–400	—	0	—	—	—	2	—	—
	400–600	—	—	−5	−5	—	—	0	4
	600–800	—	—	−40	−12	—	—	7	2
3	0–200	0	−7	—	—	0	4	—	—
	200–400	—	0	−11	−10	—	3	9	12
	400–600	—	—	2	0	—	—	10	11
	600–800	—	—	17	10	—	—	23	17
4	0–200	0	0	—	−6	9	5	—	12
	200–400	—	0	0	—	—	4	0	—
	400–600	—	—	3	5	—	—	5	2
	600–800	—	—	—	16	—	—	—	4
5	0–200	0	0	—	—	5	0	—	—
	200–400	—	—	−8	−9	—	—	1	0
	400–600	—	—	−16	−13	—	—	9	8
	600–800	—	—	−20	−18	—	—	21	18
6	0–200	0	0	3	—	11	9	11	—
	200–400	—	13	3	3	—	8	5	13
	400–600	—	—	−6	3	—	—	1	0
	600–800	—	—	−55	−6	—	—	10	3
7	0–200	0	0	−5	—	10	9	0	—
	200–400	—	—	—	0	—	—	—	2
	400–600	—	—	24	—	—	—	16	—
	600–800	—	—	31	22	—	—	20	18
8	0–200	0	0	−3	—	3	2	0	—
	200–400	—	—	0	−5	—	—	8	4
	400–600	—	—	—	14	—	—	—	12
	600–800	—	—	—	—	—	—	—	—
9	0–200	0	0	−4	—	7	6	0	—
	200–400	—	—	−4	−6	—	—	10	5
	400–600	—	—	12	18	—	—	13	14
	600–800	—	—	30	18	—	—	18	17
10	0–200	3	3	—	—	20	19	—	—
	200–400	3	3	0	—	4	0	3	—
	400–600	—	—	−2	−3	—	—	2	3
	600–800	—	—	—	—	—	—	—	—
11	0–200	−5	−6	−25	—	13	12	10	—
	200–400	—	—	−5	−20	—	—	4	9
	400–600	—	—	8	−20	—	—	1	2
	600–800	—	—	—	−6	—	—	—	0
12	0–200	−8	−12	—	—	3	1	—	—
	200–400	—	8	−14	50	—	7	0	2
	400–600	−28	−28	−17	—	12	7	3	—
	600–800	—	−28	—	—	—	12	—	—
13	0–200	−3	−4	—	—	9	11	—	—
	200–400	—	0	2	—	—	6	0	—
	400–600	36	—	37	−5	14	—	5	5
	600–800	44	37	−25	34	15	13	10	14
14	0–200	0	−4	−7	—	11	7	11	—
	200–400	—	21	−7	−2	—	9	1	7
	400–600	—	29	0	−2	—	10	4	0
	600–800	—	—	39	−2	—	—	10	4

Continued.

TABLE 2—*Continued*

Event No.	Time (sec)	Azimuthal Deviations*				Power Levels†			
		At 40 sec (deg)	At 33 sec (deg)	At 25 sec (deg)	At 20 sec (deg)	At 40 sec (db)	At 33 sec (db)	At 25 sec (db)	At 20 sec (db)
15	0–200	0	−4	−9	—	14	8	0	—
	200–400	—	—	6	−10	—	—	6	1
	400–600	—	—	—	0	—	—	—	7
	600–800	—	—	26	26	—	—	14	10
16	0–200	0	0	0	—	4	2	7	—
	200–400	25	13	−5	−10	8	6	2	5
	400–600	25	13	7	−10	12	3	0	5
	600–800	25	25	25	−10	10	8	5	7
17	0–200	10	10	7	—	12	11	19	—
	200–400	—	10	7	5	—	11	7	8
	400–600	—	—	—	5	—	—	—	0
	600–800	—	—	—	−17	—	—	—	8
18	0–200	0	2	—	—	9	3	—	—
	200–400	—	—	2	3	—	—	0	0
	400–600	—	—	27	7	—	—	14	13
	600–800	—	—	37	—	—	—	17	—
19	0–200	0	0	—	—	6	0	—	—
	200–400	0	0	2	−6	5	8	7	11
	400–600	2	2	−6	−6	1	4	2	9
	600–800	—	—	−6	−8	—	—	1	5
20	0–200	0	0	—	—	7	20	—	—
	200–400	0	0	0	0	10	3	0	8
	400–600	—	—	0	0	—	—	9	0
	600–800	—	—	−34	−23	—	—	16	18
21	0–200	0	−5	−7	—	13	6	5	—
	200–400	—	—	−11	−9	—	—	3	0
	400–600	—	—	—	—	—	—	—	—
	600–800	—	—	—	—	—	—	—	—
22	0–200	0	0	3	—	9	6	13	—
	200–400	—	—	3	3	—	—	0	11
	400–600	—	—	—	10	—	—	—	4
	600–800	—	—	—	10	—	—	—	8
23	0–200	0	0	0	—	6	4	0	—
	200–400	—	—	−29	−29	—	—	7	1
	400–600	—	—	−39	−39	—	—	4	10
	600–800	—	—	−39	−39	—	—	13	14
24	0–200	0	0	7	13	7	5	0	4
	200–400	—	—	—	15	—	—	—	10
	400–600	—	—	—	—	—	—	—	—
	600–800	—	—	—	—	—	—	—	—
25	0–200	0	−5	—	—	5	0	—	—
	200–400	—	10	−12	−19	—	9	0	6
	400–600	—	—	3	3	—	—	5	2
	600–800	—	—	10	10	—	—	8	8
26	0–200	0	0	—	—	14	13	—	—
	200–400	—	0	0	6	—	10	2	0
	400–600	—	—	—	6	—	—	—	14
	600–800	—	—	—	—	—	—	—	—

* Power levels in db relative to maximum power.

† Azimuthal deviations are differences between measured azimuth of arrival and true azimuth of epicenter of event.

Propagation Paths

The experimental results presented in Table 2 will now be used to make conjectures concerning the actual propagation paths for the various groups. It should be made emphatically clear that the data in Table 2 are insufficient to determine unequivocally the propagation paths. Thus, the results to be presented represent guesses about the

actual structure of the propagation paths. However it is believed that there is sufficient evidence to support these conjectures as being reasonably accurate indications of actual propagation paths.

As mentioned previously, the propagation paths must satisfy Fermat's principle; that is, the ray path must be a stationary-time path. This means that for Rayleigh waves the paths for the initial group arrivals will be minimum-time paths, while later group arrivals propagate along paths which, while not minimum-time paths, are sta-

TABLE 3

VARIATION IN AZIMUTH OF ARRIVAL OF RAYLEIGH WAVES AT LASA

Event No.	Azimuth (deg)	Azimuthal Variation (deg)	Azimuthal Difference (deg)
1	311.5	300–342	42
2	340.7	301–341	40
3	144.5	134–172	38
4	29.1	23–45	22
5	168.0	148–168	20
6	356.7	302–10	68
7	310.3	305–341	36
8	243.3	238–257	29
9	303.5	298–334	36
10	99.7	97–103	6
11	321.1	296–329	33
12	146.8	119–197	78
13	347.9	323–32	69
14	295.1	288–334	46
15	308.6	299–335	36
16	113.9	104–139	35
17	93.3	76–103	27
18	98.0	98–135	37
19	147.2	139–149	10
20	22.9	349–23	34
21	194.0	183–194	11
22	267.4	267–277	10
23	189.2	150–189	39
24	183.1	183–198	15
25	312.0	293–322	29
26	211.7	212–218	6

tionary-time paths. In addition, the propagation paths must satisfy Snell's Law for refraction and reflection at boundaries across which there is a contrast in phase velocity. In terms of propagation of Rayleigh waves in the surface layers of the Earth, these boundaries usually represent the continental margins. Thus, when an angle of arrival is measured which differs from the true azimuth of an event, it is quite likely that this bending of the propagation path can be explained by the refractions and reflections which must take place at continental margins. However, in some cases the bending of the ray paths appears to be caused by other major tectonic features of the Earth, such as ridges.

The data of Table 2 provide not only angles of arrival but also time delays between groups of the same frequency. These group delays enable us to determine path length differences for the multiple propagation paths traveled by a specific frequency group in

the following way. Since these group delays are measured in multiples of 200 sec, or 3.33 min, we have

$$(3.33)(K) \cong \frac{\Delta_{2,o} - \Delta_{1,o}}{U_o} + \frac{\Delta_{2,c} - \Delta_{1,c}}{U_c}$$

where K is either one, two, or three, depending on the observed group delay; U_o and U_c are the oceanic and continental group velocities, respectively, in degrees per minute; $\Delta_{2,o}$ and $\Delta_{2,c}$ are the path lengths, for the later group, contained in the oceanic and continental regions, respectively, in degrees; and $\Delta_{1,o}$ and $\Delta_{1,c}$ are defined similarly for the earlier group arrival. We can write the above equation as

$$(3.33U_o)(K) \cong \Delta + U_o(\Delta_{2,c} - \Delta_{1,c})\left(\frac{1}{U_c} - \frac{1}{U_o}\right)$$

where $\Delta = (\Delta_{2,o} - \Delta_{1,o}) + (\Delta_{2,c} - \Delta_{1,c})$ is the path length difference. In order to obtain a working formula we take 2°/min as an approximation for U_o so that

$$\Delta \cong (6.7)(K) - 2T_c$$

where T_c is the time in minutes gained by traveling a distance $(\Delta_{2,c} - \Delta_{1,c})$ over an oceanic path rather than a continental path, i.e.,

$$T_c = (\Delta_{2,c} - \Delta_{1,c})\left(\frac{1}{U_c} - \frac{1}{U_o}\right).$$

The time T_c is given in Figure 10 for the various frequency groups and for $(\Delta_{2,c} - \Delta_{1,c})$ between zero and 60°. Thus, suppose that we observe a 25-sec period group arriving from the true azimuth, and then 200 sec later another 25-sec period group arriving from a different azimuth. We have $K = 1$ and $\Delta_{1,c}$ can be measured from a map such as shown in Figure 12. If another path is hypothesized, whose angle of approach at LASA agrees with the measurement, then $\Delta_{2,c}$ can be measured for it in the same manner as was done for $\Delta_{1,c}$. Suppose $\Delta_{2,c} - \Delta_{1,c}$ is 10°, then according to Figure 10 T_c is about 1 min and $\Delta \cong 4.7°$. Hence, the path length difference for the two paths should be about 4.7°. If the second path length does not satisfy this constraint then it must be discarded and a new path found which will satisfy the conditions of the measurement. It is this trial-and-error procedure which is used to determine the propagation paths. In many cases $\Delta_{2,c} \cong \Delta_{1,c}$ so that the path length difference will be about 6.7° for each 200 sec of delay measured between the times of arrival of the groups. This latter procedure can usually be used in most cases with very little error.

It should be noted that the initial groups will usually arrive at the true azimuth or at slight azimuthal deviations from this. Thus, initially the path will consist of the great circle path between the epicenter and LASA, or a slightly refracted version of this path. Once this initial path is known the later paths can be obtained by choosing one which fits the path length difference condition and has an angle of approach at LASA which agrees with the measured angle. In most cases these later paths can be associated with refractions and reflections at the continental margins.

Six examples of such propagation paths which were similar to or typical of the results for the rest of the 26 events analyzed are shown in Figures 18 to 23. The timing se-

quence for the group arrivals is not shown in any of these figures, for simplicity. However, this information can be obtained from Table 2. In addition, two propagation paths whose azimuthal angles of arrival at LASA are within 3° of each other are usually merged into a single path. All propagation paths in these figures are drawn as straight-line segments, again for simplicity. In addition, all refractions and reflections are depicted as taking place at the geographic boundaries for the continents although it is

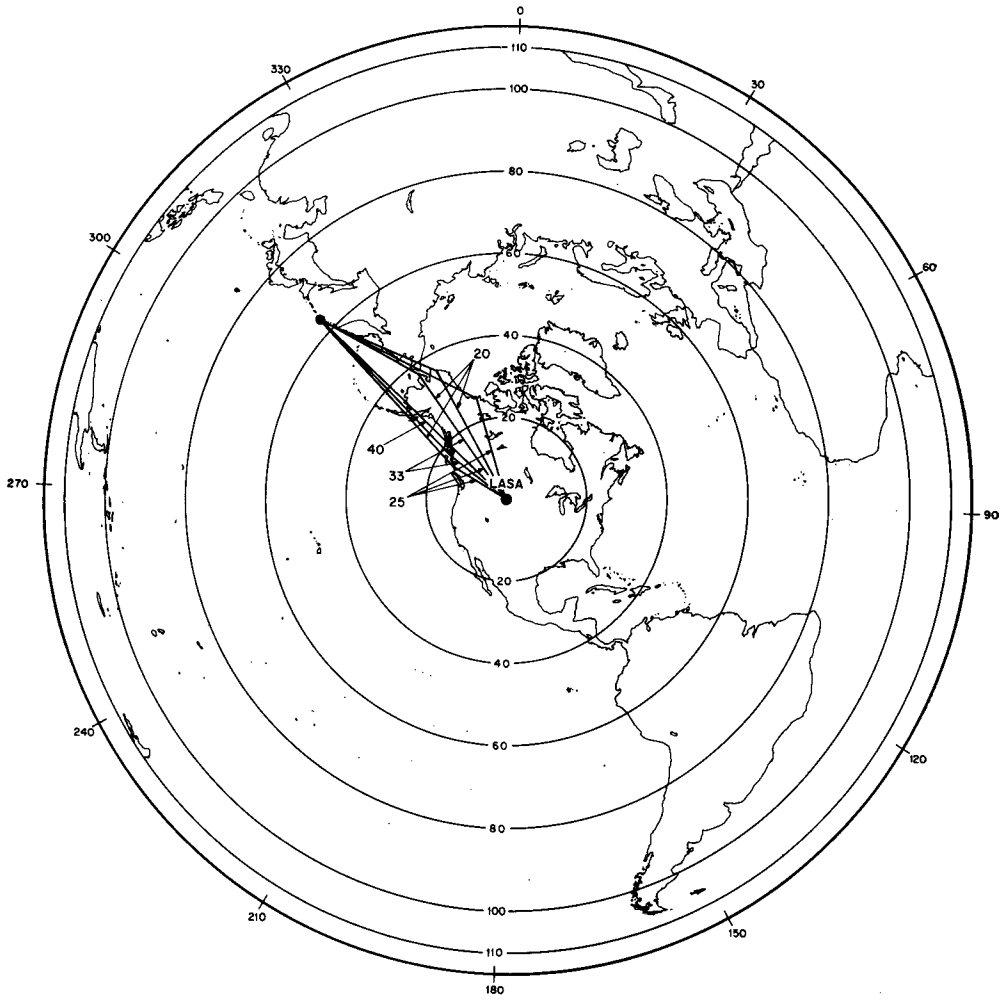

FIG. 18. Propagation paths for the Kurile Islands event no. 1 of November 21 1966.

more likely to take place at the continental margins. The difference in positions of these two boundaries is in most cases very small and may be neglected. Only one refraction or reflection is taken into account on each epicenter-to-LASA path.

The propagation paths for event no. 1 located in the Kurile Islands are shown in Figure 18. We see that initially the longer-period groups arrive at LASA along the great circle path between LASA and the epicenter, or slightly refracted versions of this path. These groups are followed by shorter-period groups which are refracted and reflected at the continental margin. The results of Figure 18 were typical of those for events nos. 7, 9, 11, 14, 15, 25. The results of Figure 20 for event no. 8 located in the Tonga Islands

are also interesting. Once more the longer-period waves arrive along the great circle path, followed by shorter-period groups arriving along slightly refracted paths. However, there appears to be a later 20-sec period group arrival which is refracted in the vicinity of the Islands of Hawaii. McGarr (1969) has also observed surface-wave refraction effects in the region near Hawaii.

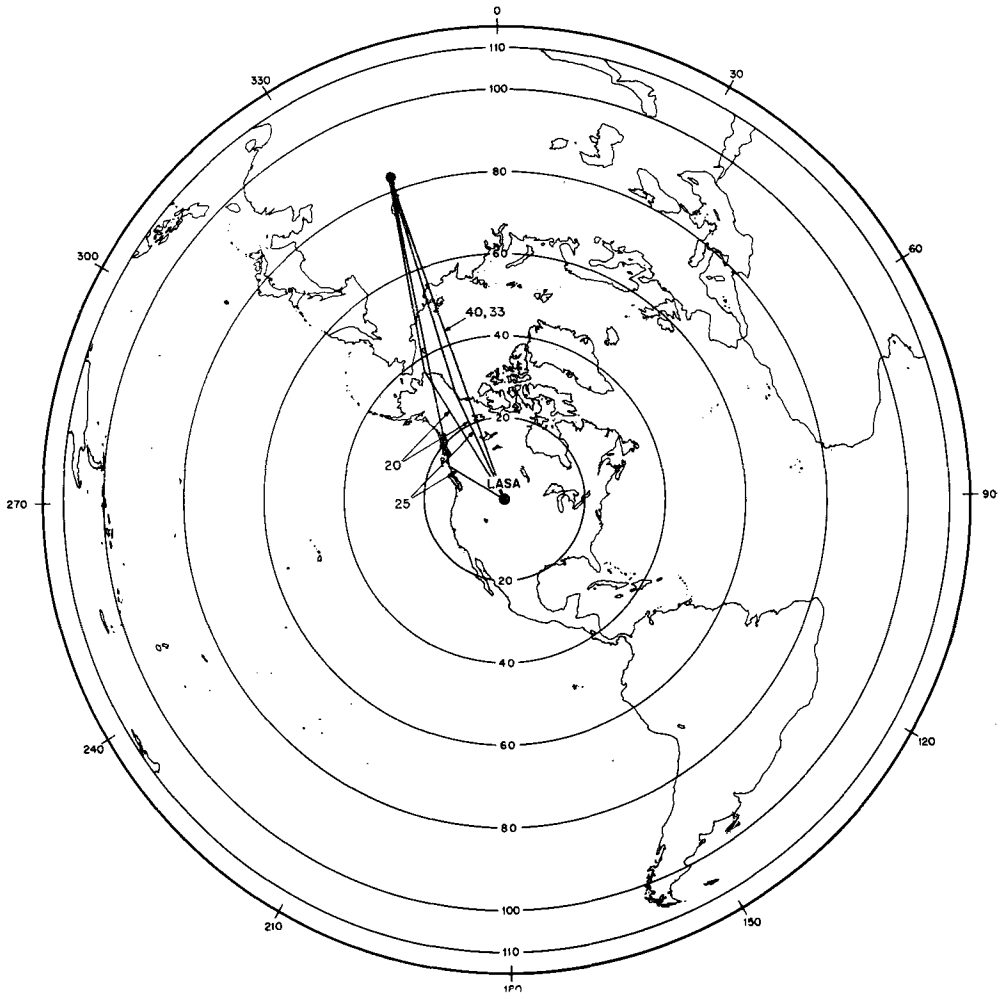

FIG. 19. Propagation paths for the Mongolia event no. 2 of January 20 1967.

In Figure 23 we see the propagation paths for event no. 17 located in the Central Mid-Atlantic Ridge. In this case the longer-period groups arrive from an angle which deviates from the true azimuth by about 10°. It appears that these groups are guided by the mid-Atlantic ridge and then emerge from it at the point where the ridge makes a sharp turn away from the direction toward LASA. The shorter-period groups do not appear to be guided by the ridge, but are refracted and reflected in the usual way. These results were typical of those found for events nos. 10 and 18.

It should be noted that reflection of a group usually takes place at a continent-to-

ocean boundary and that the angle of incidence usually exceeds the critical angle for the period of the group. This can be seen by comparing Figure 11, which shows the critical angle versus period, with Figures 18 to 23. This result is to be expected, since it is at these angles of incidence that reflection of large amounts of energy would be expected.

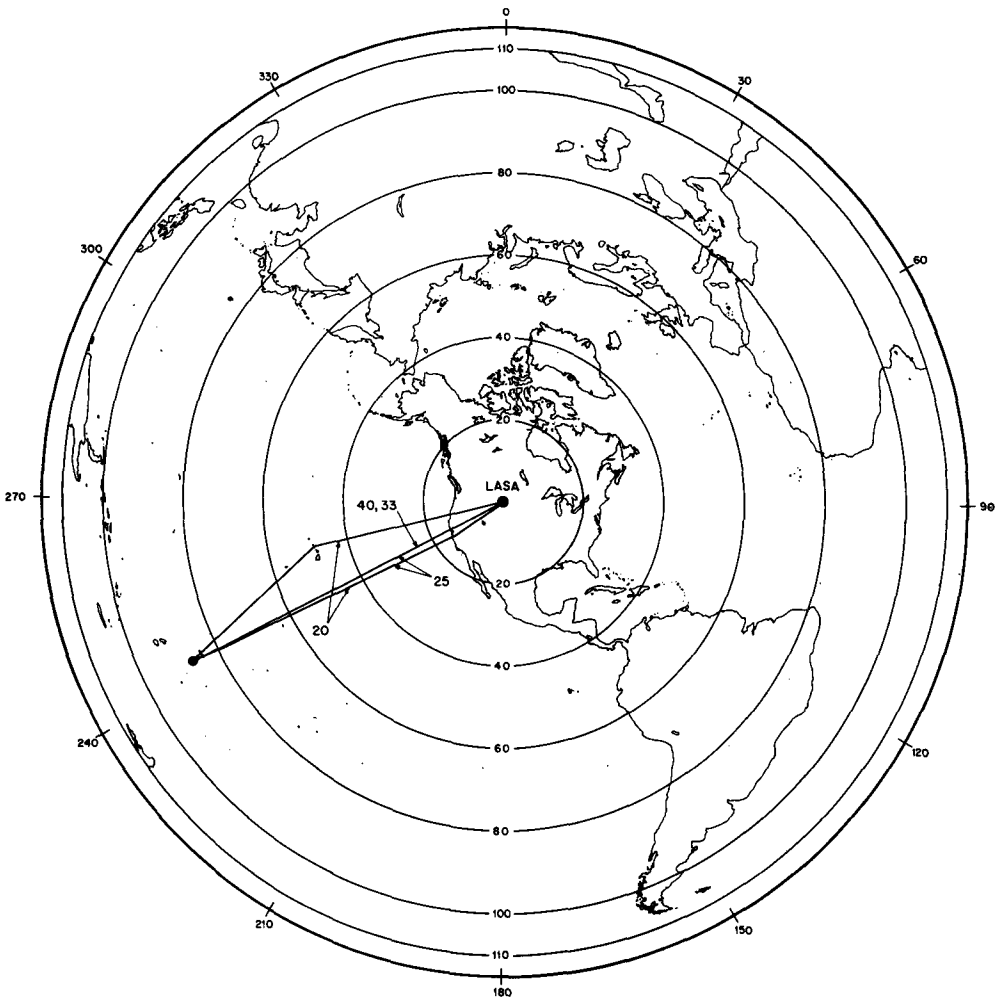

FIG. 20. Propagation paths for the Tonga Islands event no. 8 of June 14 1967.

CONCLUSIONS

The analysis of Rayleigh-wave multipath propagation has been performed at LASA using the HR method. This has allowed a greater angular resolution and accuracy to be attained than was previously possible. In addition, this improved resolution and accuracy has been obtained for several frequency groups which have been found to be important for seismic discrimination based on the $M_s - m_b$ criterion.

The experimental results indicate that in the 20- to 40-sec period range the multipath propagation is caused primarily by the phase-velocity contrast between oceanic and continental regions which leads to refractions and reflections at the continental mar-

gins. The analysis provided information about path length differences. This in turn has enabled us to make reasonably good conjectures about the actual propagation paths. In almost all cases for the 26 events analyzed, these propagation paths could be associated with refractions and reflections at the continental margins. It is interesting that the reflection of a group usually takes place at a continent-to-ocean boundary and the angle of incidence usually exceeds the critical angle for the period of the group.

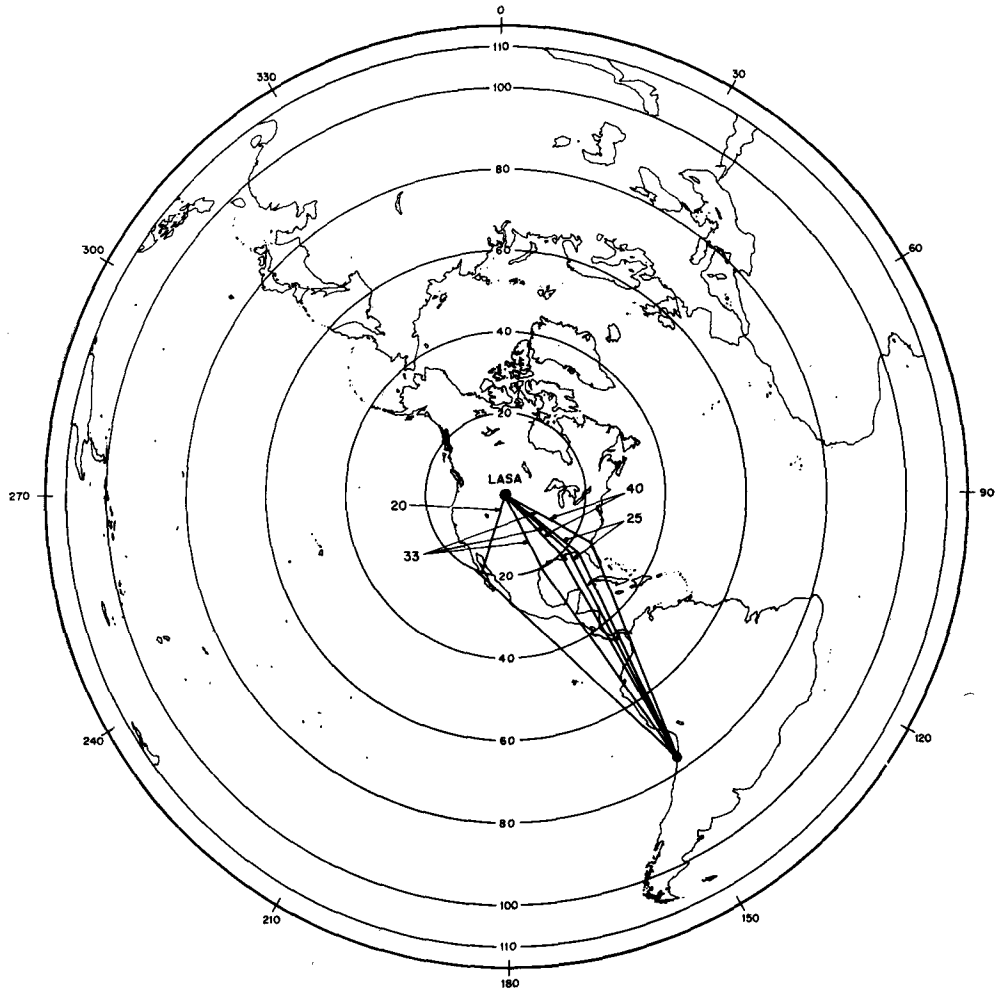

FIG. 21. Propagation paths for the Northern Chile event no. 12 of September 8 1967.

There were some exceptions, however, in which the multipath propagation was caused by other major tectonic features of the Earth, such as ridges (*cf.* Figure 23). In addition, for event no. 5 the shorter-period wave groups did not travel the great circle path between LASA and the epicenter but traveled along a path which was bent toward the east. This phenomenon may be caused by a phase-velocity contrast between the western and eastern parts of the United States and Mexico (*cf.* Table 2).

The present results indicate that the multipath propagation phenomenon for Ray-

leigh waves is quite complex. Thus, if the multipath propagation is known for a given epicenter, it appears that it would be difficult to predict this effect for an epicenter whose location is significantly different from that of the given epicenter. The experimental results indicate that the multipath propagation may be significantly different for events whose epicenters are located within 5° of each other. This has important applications to the problem of matched filtering of Rayleigh waves (*cf.* Capon et al.,

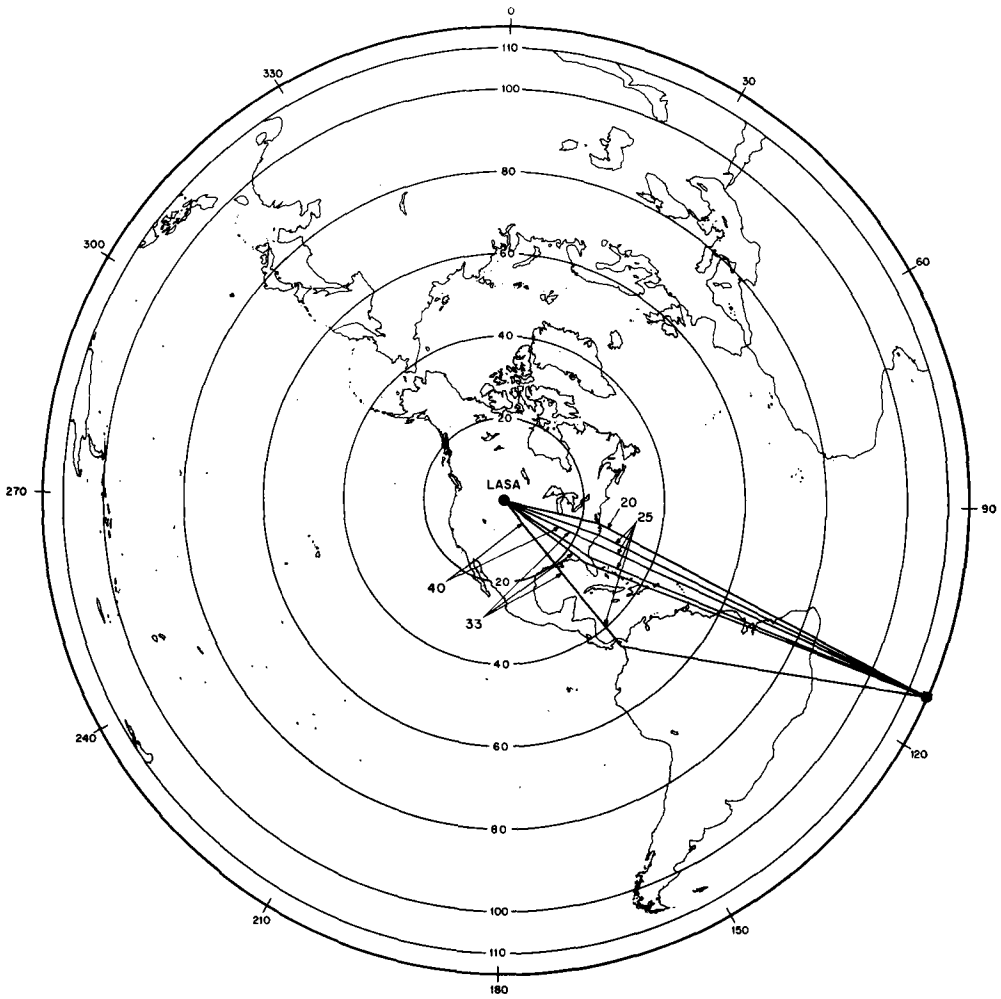

FIG. 22. Propagation paths for Tristan Da Cunha event no. 16 of September 20 1967.

1969). If the matched filtering is to be done by using the wave form of a master event as the impulse response of the matched filter, then a large number of such master events would have to be used due to the inability to predict the multipath propagation phenomenon for Rayleigh waves of events whose epicenters are located within about 5° of each other. Thus, the use of chirp wave forms for matched filtering, as recommended by Capon *et al.* (1969), may represent the most reasonable approach to the problem of matched filtering of Rayleigh waves.

Acknowledgment

The author would like to thank Dr. Bruce Julian for helpful discussions concerning the interpretation of the experimental results and Dr. Authur C. Tarr of the U. S. Coast and Geodetic Survey for supplying the equidistant azimuthal projection map for LASA. In addition, the author is indebted to the referee for several helpful comments.

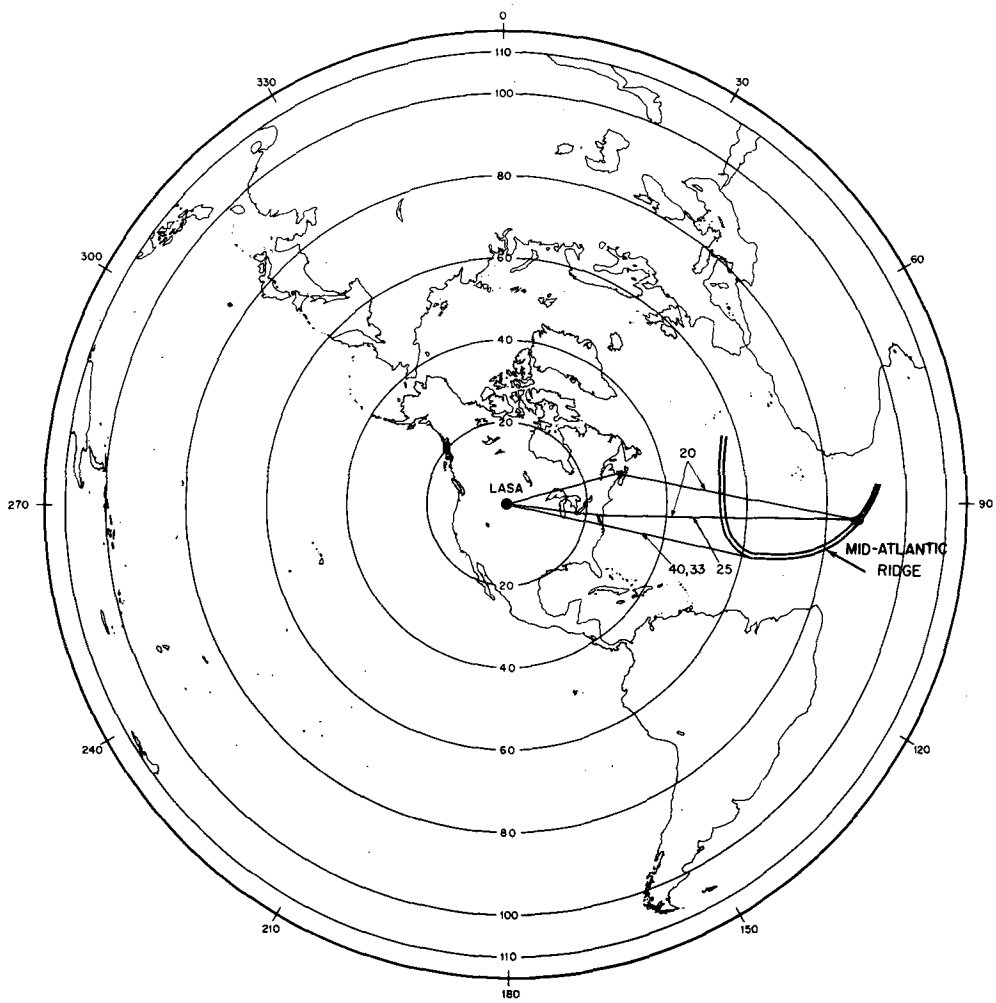

Fig. 23. Propagation paths for Central Mid-Atlantic Ridge event no. 17 of September 22 1967.

References

Ben-Menaham, A. and D. G. Harkrider (1964). Radiation patterns of seismic surface waves from buried dipolar point sources in a flat stratified earth, *J. Geophys. Res.* **69**, 2605–2620.

Blackman, R. B. and J. W. Tukey (1959). *The Measurement of Power Spectra from the Point of View of Communications Engineering*, Dover Publications, New York.

Brune, J. N., A. Espinosa, and J. Oliver (1963). Relative excitation of surface waves by earthquakes and underground explosions in the California-Nevada region, *J. Geophys. Res.* **68**, 3501–3513.

Bullen, K. E. (1963). *An Introduction to the Theory of Seismology*, Cambridge University Press, New York.

Capon, J., R. J. Greenfield, and R. T. Lacoss (1969). Long-period signal processing results for the large aperture seismic array, *Geophysics* **34**, 305–329.

Capon, J. (1969a). Investigation of long-period noise at the large aperture seismic array, *J. Geophys. Res.* **74**, 3182–3194.

Capon, J. (1969b). High-resolution frequency-wavenumber spectrum analysis, *Proc. IEEE* **57**, 1408–1418.

Evernden, J. F. (1953). Direction of approach of Rayleigh waves and related problems, Part I, *Bull. Seism. Soc. Am.* **43**, 335–374.

Evernden, J. F. (1954). Direction of approach of Rayleigh waves and related problems, Part II, *Bull. Seism. Soc. Am.* **44**, 159–184.

Ewing, M., W. S. Jardetsky, and F. Press (1957). *Elastic Waves in Layered Media*, McGraw-Hill Book, New York.

Green, P. E., R. A. Frosch, and C. F. Romney (1965). Principles of an experimental large aperture seismic array (LASA), *Proc. IEEE* **53**, 1821–1833.

Gutenberg, B. (1945). Amplitudes of surface waves and magnitudes of shallow earthquakes, *Bull. Seism. Soc. Am.* **35**, 3–12.

Gutenberg, B. and C. F. Richter (1956). Magnitude and energy of earthquakes, *Ann. Geophys.* **9**, 1–14.

Harkrider, D. G. (1964). Surface waves in multilayered elastic media. I. Rayleigh and Love waves from buried point sources in a multilayered elastic half-space, *Bull. Seism. Soc. Am.* **54**, 627–679.

Knopoff, L., S. Mueller, and W. L. Pilant (1966). Structure of the crust and upper mantle in the Alps from the phase velocity of Rayleigh waves, *Bull. Seism. Soc. Am.* **56**, 1009–1044.

Liebermann, R. C., C. Y. King, J. N. Brune, and P. W. Pomeroy (1966). Excitation of surface waves by the underground nuclear explosion Longshot, *J. Geophys. Res.* **71**, 4333–4339.

Liebermann, R. C. and P. W. Pomeroy (1969). Relative excitation of surface waves by earthquakes and underground explosions, *J. Geophys. Res.* **74**, 1575–1590.

Mal, A. K. and L. Knopoff (1965). Transmission of Rayleigh waves past a step change in elevation, *Bull. Seism. Soc. Am.* **55**, 319–334.

Marshall, P. D., E. W. Carpenter, A. Douglas, and J. B. Young (1966). Some seismic results of the Longshot explosion, Atomic Weapons Research Establishment, *U. K. Atomic Energy Authority Report 0-67/66*.

McGarr, A. (1969). Amplitude variations of Rayleigh waves-horizontal refractions, *Bull. Seism. Soc. Am.* **59**, 1307–1334.

McGarr, A. and L. E. Alsop (1967). Transmission and reflection of Rayleigh waves at vertical boundaries, *J. Geophys. Res.* **72**, 2169–2180.

Oliver, J. (1962). A summary of observed seismic surface wave dispersion, *Bull. Seism. Soc. Am.* **52**, 81–86.

Pilant, W. L. and L. Knopoff (1964). Observations of multiple seismic events, *Bull. Seism. Soc. Am.* **54**, 19–39.

Press, F., G. Dewart, and R. Gilman (1963). A study of diagnostic techniques for identifying earthqukes, *J. Geophys. Res.* **68**, 2909–2928.

Lincoln Laboratory
Massachusetts Institute of Technology
Lexington, Massachusetts

Manuscript received April 30 1970